AFWL-TR-75-342, Vol. II

AFWL-TR-
75-342
Vol. II

AD A032454

2 NW

LASER BEAM TARGET INTERACTION

Volume II
Laser Effects at 10.6 Microns

The Boeing Company
Seattle, WA 98124

July 1976

Final Report

DDC
RECEIVED
NOV 24 1976
C

Approved for public release; distribution unlimited.

Prepared for
ADVANCED RESEARCH PROJECTS AGENCY
1400 Wilson Blvd.
Arlington, VA 22209

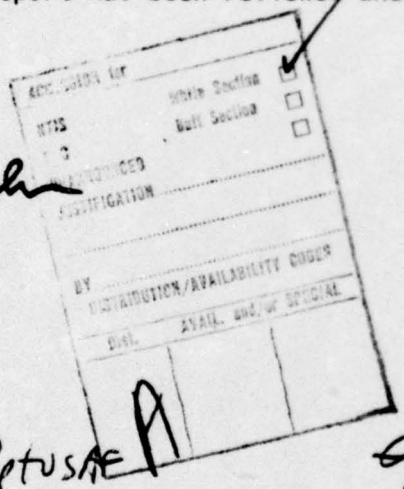
AIR FORCE WEAPONS LABORATORY
Air Force Systems Command
Kirtland Air Force Base, NM 87117

This final report was prepared by The Boeing Company, Seattle, Washington, under Contract F29601-73-A-0038-0002, Job Order 19051006, with the Air Force Weapons Laboratory, Kirtland Air Force Base, New Mexico. Dr. Ralph R. Rudder (PGV) was the Laboratory Project Officer-in-Charge.

When US Government drawings, specifications, or other data are used for any purpose other than a definitely related Government procurement operation, the Government thereby incurs no responsibility nor any obligation whatsoever, and the fact that the Government may have formulated, furnished, or in any way supplied the said drawings, specifications, or other data, is not to be regarded by implication or otherwise, as in any manner licensing the holder or any other person or corporation, or conveying any rights or permission to manufacture, use, or sell any patented invention that may in any way be related thereto.

This report has been reviewed by the Information Office (OI) and is releaseable to the National Technical Information Service (NTIS). At NTIS, it will be available to the general public, including foreign nations.

This technical report has been reviewed and is approved for publication.



Ralph R. Rudder
RALPH R. RUDDER
Project Officer

David Evans Capt USAF
for HECTOR REDE
Major, USAF
Chief, Effects and Vulnerability Branch

Louis H. Bernasconi
LOUIS H. BERNASCONI
Colonel, USAF
Chief, LEAPS Division

DO NOT RETURN THIS COPY. RETAIN OR DESTROY.

UNCLASSIFIED

SECURITY CLASSIFICATION OF THIS PAGE (When Data Entered)

REPORT DOCUMENTATION PAGE

READ INSTRUCTIONS BEFORE COMPLETING FORM

1. REPORT NUMBER: AFWL-TR-75-342, Vol. II

2. GOVT ACCESSION NO.

3. RECIPIENT'S CATALOG NUMBER

4. TITLE (and Subtitle): LASER BEAM TARGET INTERACTION. Volume II, Laser Effects at 10.6 Microns.

5. TYPE OF REPORT & PERIOD COVERED: Final Report. 31 Mar 74 - 15 Jan 76

6. PERFORMING ORG. REPORT NUMBER

7. AUTHOR(s): R. B. Hall, P. S. P. Wei, W. E. Maher

8. CONTRACT OR GRANT NUMBER(s): F29601-73-A-0038-0002, ARPA Order - 1905

9. PERFORMING ORGANIZATION NAME AND ADDRESS
The Boeing Aerospace Company
P. O. Box 3999
Seattle, WA 91824

10. PROGRAM ELEMENT, PROJECT, TASK AREA & WORK UNIT NUMBERS
62301E
19051006

11. CONTROLLING OFFICE NAME AND ADDRESS
Advanced Research Projects Agency
1400 Wilson Blvd.
Arlington, VA 22209

12. REPORT DATE: Jul 76

13. NUMBER OF PAGES: 74

14. MONITORING AGENCY NAME & ADDRESS (if different from Controlling Office)
Air Force Weapons Laboratory (PGV)
Kirtland Air Force Base, NM 87117

15. SECURITY CLASS. (of this report): UNCLASSIFIED

15a. DECLASSIFICATION/DOWNGRADING SCHEDULE

16. DISTRIBUTION STATEMENT (of this Report)

D180-19256-2

Approved for public release; distribution unlimited.

1905 10

17. DISTRIBUTION STATEMENT (of the abstract entered in Block 20, if different from Report)

AFWL TR-75-342-Vol-2

18. SUPPLEMENTARY NOTES

19. KEY WORDS (Continue on reverse side if necessary and identify by block number)

Laser Beam Target Interaction	Pulsed CO_2 laser
Threshold intensity	LSD waves
Spatial dependence	Target plasmas
Absorbed energy	Spectroscopic and interferometric diagnostics

20. ABSTRACT (Continue on reverse side if necessary and identify by block number)

This report is the second of two volumes on the subject of Laser Beam Target Interaction. Volume I considered both the performance and design of a pulsed chemical laser and the laser effects measurements made with that laser. This volume describes both impulse and thermal coupling measurements made at 10.6 microns wavelength. The laser used was the Boeing double-pulse Marx Bank laser which can emit two 15 joule pulses with any desired pulse separation (from simultaneous to several seconds). Spectroscopic measurements were used

(over)

DD FORM 1 JAN 73 1473 EDITION OF 1 NOV 65 IS OBSOLETE

UNCLASSIFIED

SECURITY CLASSIFICATION OF THIS PAGE (When Data Entered)

059610

ABSTRACT (cont'd)

to determine some of the basic properties of laser-supported absorption waves. In addition, however, a limited amount of data was gathered in order to determine the threshold intensity for igniting laser-supported absorption (LSA) waves from magnesium. The main goal of the work reported here was to determine impulse coupling and thermal coupling at high intensities. One of the most important results was to determine the spatial dependence of absorbed energy on a target at high laser intensities.

Preface

This report was prepared by The Boeing Aerospace Company under Contract F29601-73-A-0038-0002. The research was performed under Project F29601-74-10066, and was funded by the Advanced Research Projects Agency under ARPA Order 1905.

Inclusive dates of research were March 31, 1974 to January 15, 1976.

The authors are pleased to acknowledge the excellent assistance of L. Alexander.

The contractor report number is D180-19256-2.

TABLE OF CONTENTS

Section		Page
I	INTRODUCTION	1
II	DOUBLE-PULSE CO_2 FACILITY	3
III	SPECTROSCOPIC INVESTIGATIONS	8
	1. Visible Spectrum as a Function of Time	8
	2. Time Dependence of Two Emission Lines	13
IV	DOUBLE-PULSE LSA WAVE IGNITION THRESHOLDS ON MAGNESIUM	16
V	IMPULSE ON TARGETS AND AIR PRESSURE PULSES PRODUCED BY DOUBLE-PULSE CO_2 LASER PULSES	19
VI	THERMAL COUPLING MEASUREMENTS	27
	1. Basic Data	27
	2. Spot Size Dependence	32
	3. Thermal Coupling with The Separation Time as Parameter	34
	4. Pressure Dependence	37
	5. Spatial Distribution of Absorbed Energy	45
	6. Damage Model Based on Thermal Coupling Measurements	61
VII	SUMMARY	66
	References	67

21	Single Laser Pulse Thermal Coupling to Magnesium	43
22	Single Laser Pulse Thermal Coupling to 304 Stainless Steel	44
23	Laser Power as a Function of Time	48
24	Front and Rear Surface Temperature Time Dependence	50
25	Logarithmic Plot of Front and Rear Temperature Approaching Equilibrium	51
26	Temperature Profile in an Aluminum Sheet 0.028 cm Thickness. Laser Pulse Energy was 2 Joules in a Spot 2.5 mm Diameter and With a Surface Absorptivity of 0.023	52
27	Temperature Profile in an Aluminum Sheet 0.028 cm Thickness Laser Pulse Energy was 2 Joules in a Spot 2.5 mm Diameter and With a Surface Absorptivity of 0.023	53
28	Temperature Versus Time for Selected Energy Density Profiles	56
29	Comparison of Theory and Experiment for a Low Energy Laser Pulse (No Plasma Produced)	58
30	Temperature Versus Time Produced by a High-Energy Laser Pulse Which Produced a Laser-Supported Detonation Wave	60
31	Comparison of the Absorbed Energy Density Profiles Obtained Both With and Without Plasma Production	62
32	Fluence Required for Burnthrough of an 0.3 cm Aluminum Plate	64

ILLUSTRATIONS

Figure		Page
1	Schematic Diagram of the Optical Arrangement of the Double-Pulse Laser System	4
2	View of the Experimental Area	5
3	Typical Double Marx Bank CO_2 Laser Pulses	7
4	Microdensitometer Traces of Spectrum of a Plasma Produced by a CO_2 Laser Pulse on BN	9
5	Temporal Behavior of Emission Lines from the Plasma Produced by Two 15 Joule Pulses Separated by 50 μsec. The Spectrograph is Looking at 2 mm in Front of the Aluminum Target	15
6	Plasma Ignition on Magnesium Samples A and B	17
7	I/E Values Shown as a Function of Separation Time for Aluminum	21
8	I/E Values Shown as a Function of Separation Time for 304 Stainless Steel	23
9	Boeing Pressure Transducer	24
10	Pressure Transducer Measurements (10 Microseconds/Division) (a) Lucite Target Pressure Pulsed, (b) Incident Laser Pulses for (a), (c) Aluminum Target Pressure Pulse, (d) Incident Laser Pulses for (b)	25
11	Coupling Efficiency as a Function of Laser Intensity for Single 10.6 Micron Pulses	29
12	The Experimental Apparatus for Double-Pulse Thermal Coupling	30
13	Double Laser Pulse Thermal Coupling to Magnesium at 1/100 Atmosphere At and Below Plasma Threshold	31
14	Aluminum Absorption Coefficient Enhancement	33
15	Thermal Coupling to Magnesium at One Atmosphere for Two Spot Sizes	35
16	Sensitivity of Absorption Coefficient of the Separation Time	36
17	Double Laser Pulse Thermal Coupling to Magnesium at 1/100 Atmosphere	38
18	Laser Beam Thermal Coupling to Magnesium: Single and Simultaneous Double Pulses at 80 cm F.L. and One Atmosphere	39
19	Single Laser Pulse Coupling to Aluminum	40
20	Aluminum Crater Produced at Low Atmospheric Pressure	42

TABLES

Table		Page
1	Measured Velocity of Species Evaporated from Solid Surfaces	11
2	Calculated Evaporation Velocity from the Three-Dimensional Boltzmann Distribution	12
3	Corresponding Energy Density Profiles and Temperature at r = 0	55

SECTION I

INTRODUCTION

Even though a considerable amount of laser coupling data has been gathered at 10.6 microns wavelength (Refs. 1-4) there still exists an incomplete understanding of laser effects. In particular, a precise determination from first principles of laser-supported detonation (LSD) wave ignition thresholds cannot be now made. In addition, the theoretical prediction of thermal coupling under plasma ignition conditions is not now possible.

For these reasons, a series of experiments at 10.6 microns wavelength was carried out using the Boeing Double-Pulse CO_2 Laser.

Section II describes the Boeing Double-Pulse Facility and indicates the laser pulse shape and energy density profiles.

Section III describes spectroscopic measurements on the LSD wave plasma using both time-integrated and time-resolved techniques.

Section IV describes measurements of the LSA wave ignition threshold using double pulses where magnesium is the target material. It was found that the ignition threshold was dependent on the temporal separation between the double laser pulses as well as the total double pulse energy.

The impulse on targets of aluminum, stainless steel, and titanium was measured with the double-pulse CO_2 laser as a function of the pulse separation time. These measurements, reported in Section V, showed that only a very small increase of the impulse can be obtained by proper temporal spacing of two laser pulses. This occurs because most of the impulse is caused by the air blast wave. As a result, the total impulse is reduced if the second of the two pulses occurs before the ambient gas density is restored to the target surface.

Section VI describes the thermal coupling of laser energy on solid targets which is the main effort of this study. The results tend to show that laser spot size is not very important in determining total thermal coupling to highly reflective targets. Further measurements

were made with the double-pulse CO_2 laser on the variation of the thermal coupling coefficient with separation time and pressure. These results showed that thresholds tend to decrease slowly with increasing pressure and that, below the ignition threshold, there is a slightly increasing coupling to the target with increasing fluence. One interpretation of this trend is that the surface temperatures reached are higher indicating a true reduction in the reflectivity. The final result of these thermal coupling measurements was to determine the spatial distribution over which the total energy is added to the target. These measurements are for a single small spot size and lead to the conclusion that the plasma contribution to the thermal coupling extends over an appreciable area greatly exceeding the laser spot size itself. This fact leads to the conclusion that both total coupling and the spatial distribution must be determined in order to assess the enhanced coupling of pulsed laser devices.

SECTION II

DOUBLE PULSE CO_2 LASER FACILITY

This laboratory facility has been in existence since 1973 with the capability to produce two 10.6 μ laser pulses with an adjustable interpulse separation time (Ref. 5). The two longitudinal discharge low pressure lasers are operated with two separate Marx Capacitor Banks which, when erected, apply 420 kV to the lasers. Both the temporal behavior and the energy in each laser beam are monitored by a fast detector and a calorimeter, respectively, which receive a fraction of the energy split from the original beam by a KCl wedge. A schematic of the diagnostic arrangement is shown in figure 1.

The output beams from the lasers are used in both ambient air and in low pressure experiments. For the latter a 1 meter diameter spherical vacuum vessel is used as shown in figure 2. It has two KCl windows and focusing optics are inside of it.

In the experiments reported here, several different focal length lenses and mirrors were used. These focal lengths were 28 cm, 37.5 cm, and 80 cm and produced focal spot diameters of 2.5, 3.4, and 7.2 millimeters respectively. It was shown in reference 5 that the energy density profile of the focussed laser beam was

$$e(r) = e_o\,(1 - r^2/d^2) \text{ joules/cm}^2 \qquad (1)$$

where

r = radius from center of spot ($r<d$)
$d = 4.5 \times 10^{-3}\, f$ cm.
f = focal length (cm)

In equation 1, the maximum energy density e_o at $r = 0$ is

$$e_o = \frac{2E}{\pi d^2} \text{ joules/cm}^2 \qquad (2)$$

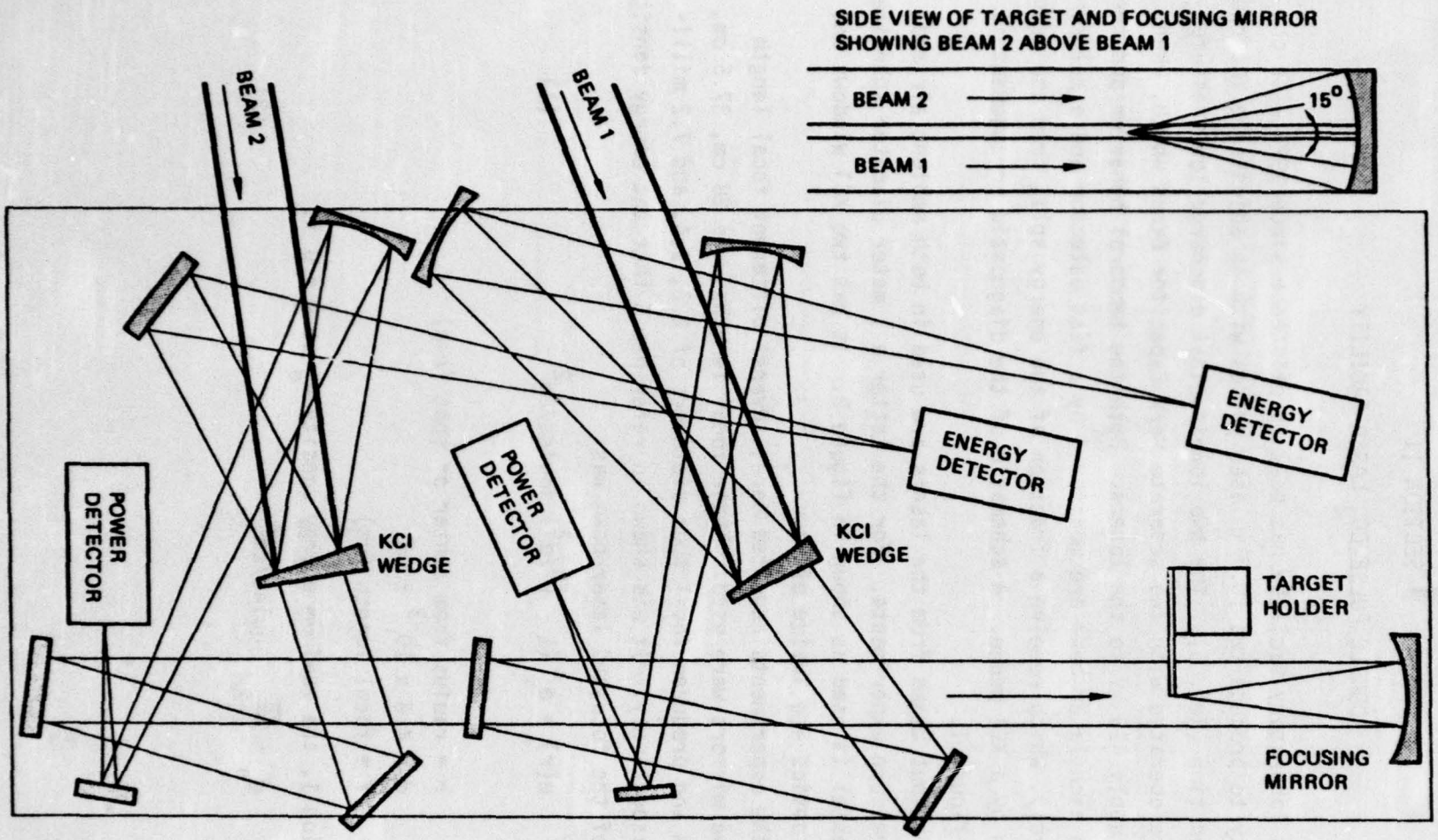


Figure 1. Schematic Diagram of the Optical Arrangement of the Double-Pulse Laser System

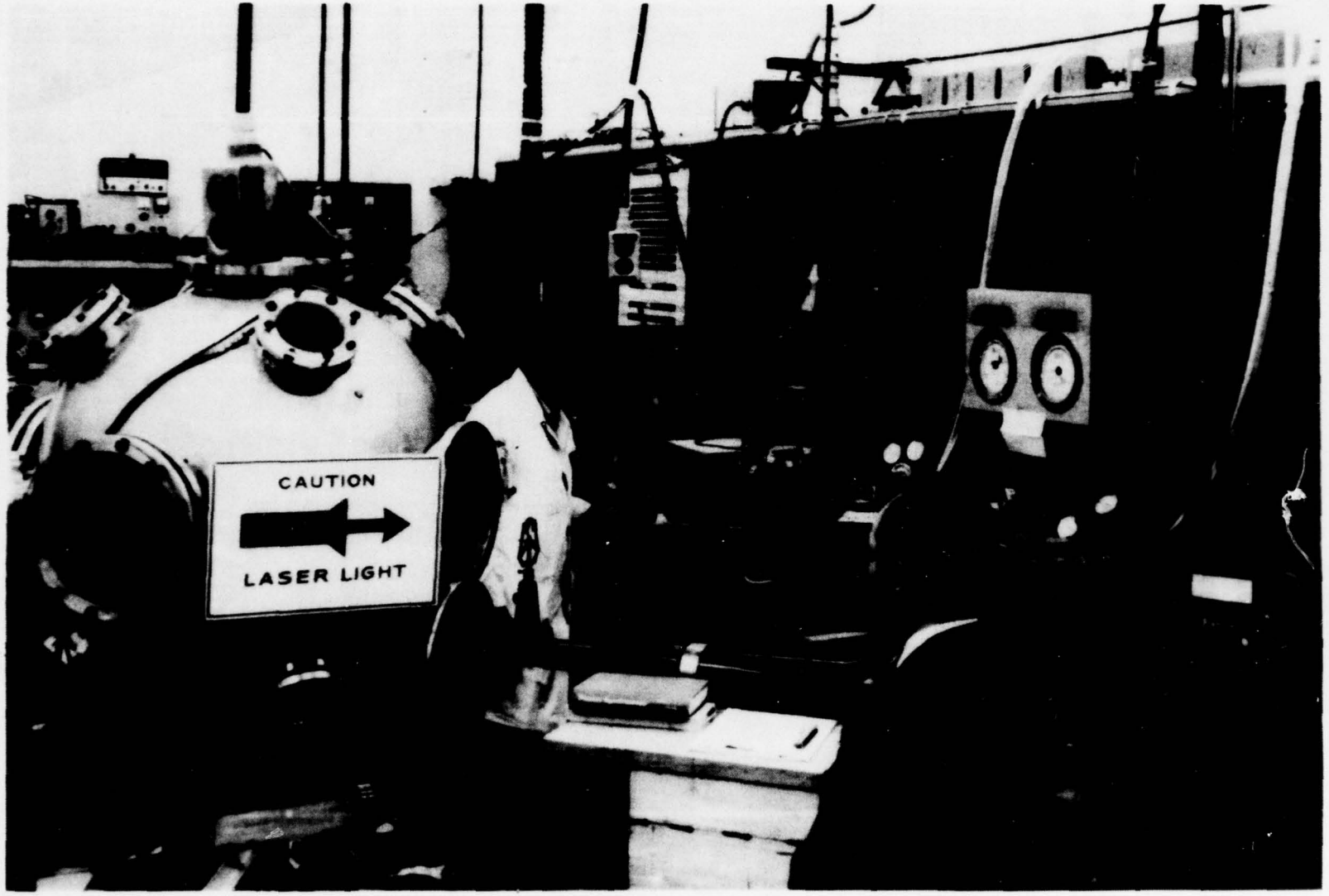


Figure 2 . View of the Experimental Area

where E is the total laser energy.

A typical double-pulse temporal profile is shown in figure 3. The ratio of the height of the front-end spike to the laser peak changes somewhat with operating conditions and the overall pulse shape may also vary. For this reason, figure 3 should not be regarded as the typical pulse shape for all the reported experiments. (A representative pulse shape for thermal coupling is shown in figure 23).

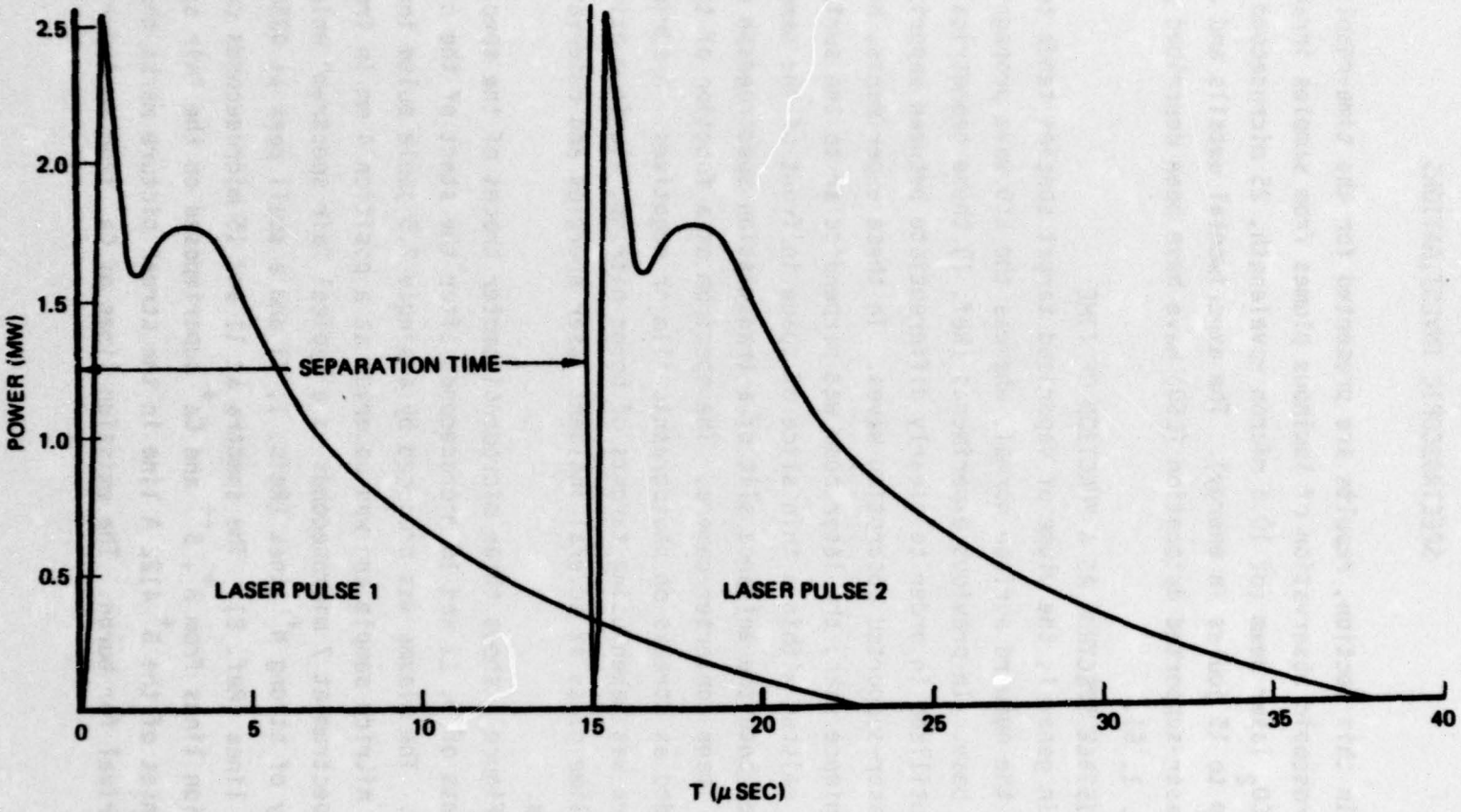


Figure 3. Typical Double Marx Bank CO_2 Laser Pulses

SECTION III
SPECTROSCOPIC INVESTIGATIONS

In this section, results are presented for the time-resolved spectroscopic observation of luminous plumes from samples irradiated by a CO_2 laser beam (of 10.6 micron wavelength, 25 microsecond duration and up to 15 joules in energy). The experimental details and a study of the laser-supported detonation (LSD) wave have been described previously (Refs. 1, 6).

1. VISIBLE SPECTRUM AS A FUNCTION OF TIME

In general, the plume of vaporized target species tends to be ejected along the outward surface normal, whereas the LSD wave propagates along the laser beam. In previous experiments (Ref. 1) these geometrical factors were utilized in order to clearly differentiate between vaporization and laser-supported absorption waves. In these experiments, however, for convenience sake, the laser beam was perpendicular to the surface. The light emitted within a thin slice of space in front of the sample was focused onto the entrance slit of a transmission spectrograph coupled to an image converter camera. The spectrum as a function of time was recorded as streaks on photographic film or negatives. A series of spectra was taken using targets of boron nitride, aluminum oxide and soda-lime glass at several incident laser energies and observation distances.

Figure 4 shows three microdensitometer traces of the spectrum at instants of 7, 11 and 15 microseconds after the start of the single laser pulse. The plasma was produced by a single 7.5 joule pulse incident on a boron nitride sample and was observed at a position 4 mm in front of it. The spectrum at 7 microseconds is a typical "air spectrum" which consists mainly of strong N^+ lines (Refs. 1, 7) and a small peak at 4350 A due to O^+ lines (Ref. 8). The spectra at 11 and 15 microseconds contain emission lines from B^+, B^{++} and Ca^+ superimposed on the "air spectrum." The onset of the B^+ 4122 A line in the streak picture marks the time of arrival for boron. The emission lines of Ca^+ from an impurity in the

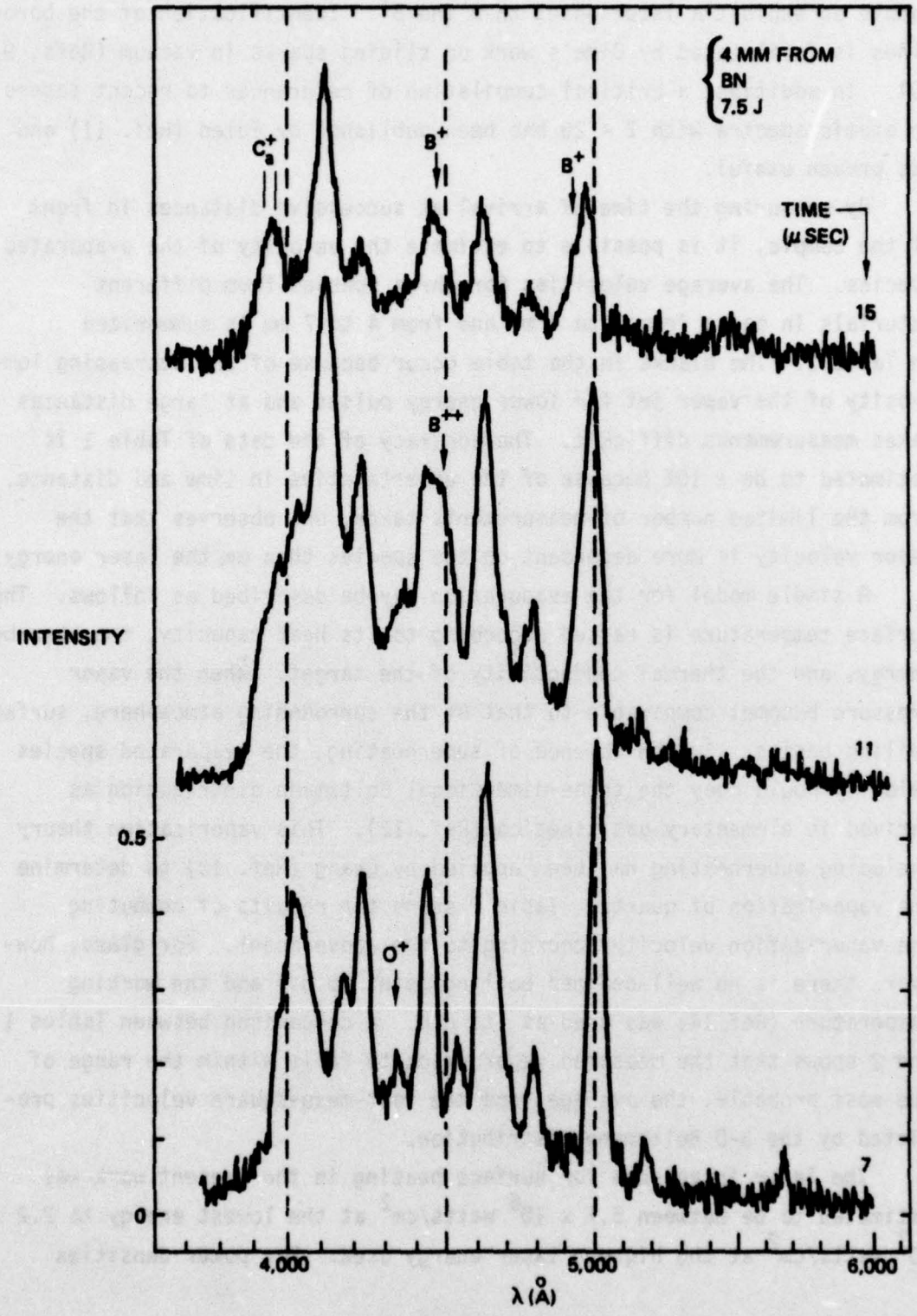


Figure 4. Microdensitometer Traces of Spectrum of a Plasma Produced By a CO_2 Laser Pulse on BN

sample do exhibit a later onset than the B^+. Identification of the boron lines is facilitated by Olme's work on sliding sparks in vacuum (Refs. 9, 10). In addition, a critical compilation of references to recent papers on atomic spectra with $Z < 28$ has been published by Edlen (Ref. 11) and has proven useful.

By measuring the time of arrival at successive distances in front of the sample, it is possible to estimate the velocity of the evaporated species. The average velocities for three species from different materials in going from 1 to 4 mm and from 4 to 7 mm is summarized in Table 1. The blanks in the table occur because of the decreasing luminosity of the vapor jet for lower energy pulses and at large distances makes measurements difficult. The accuracy of the data of Table 1 is estimated to be ± 10% because of the uncertainties in time and distance. From the limited number of measurements taken, one observes that the vapor velocity is more dependent on the species than on the laser energy.

A simple model for the evaporation may be described as follows. The surface temperature is raised according to its heat capacity, the absorbed energy, and the thermal conductivity of the target. When the vapor pressure becomes comparable to that of the surrounding atmosphere, surface boiling begins. In the absence of superheating, the evaporated species velocity would obey the three-dimensional Boltzmann distribution as derived in elementary gas kinetics (Ref. 12). This vaporization theory including superheating has been applied by Chang (Ref. 13) to determine the vaporization of quartz. Table 2 shows the results of computing the vaporization velocity according to the above model. For glass, however, there is no well-defined boiling point (b.p.) and the working temperature (Ref. 14) was used as its b.p. A comparison between Tables 1 and 2 shows that the measured vapor velocity falls within the range of the most probable, the average, and the root-mean-square velocities predicted by the 3-D Boltzmann distribution.

The laser irradiance for surface heating in the present work was estimated to be between 5.7×10^6 watts/cm^2 at the lowest energy to 2.2×10^7 watts/cm^2 at the highest laser energy used. For power densities

TABLE 1. MEASURED VELOCITY OF SPECIES EVAPORATED FROM SOLID SURFACES

Material	Emission Line (Å)	Laser Energy (J)	Arrival Time at 1 mm (μsec)	Measured Velocity (10^5 cm/sec)	
				1→4 mm	4→7 mm
BN	B^+ 4122	15	9.7	2.1[a]	---
		7.5	8.3	2.6[a]	---
		3.8	---	---	---
Al_2O_3	Al 3944	15	8.0	1.36[b]	1.44[a]
	& 3961	7.5	3.6	1.08[b]	---
		3.8	5.5	0.91[a]	---
Soda-Lime Glass	Ca^+ 3933	15	4.4	0.64[b]	0.61[a]
	& 3968	7.5	2.2	0.60[a]	0.57[a]
		3.8	2.4	0.31	---

Some velocity data presented here are averaged from more than one raw data value.

The letters a, and b denote the number of raw measurements to be 2 and 3, respectively. The accuracy is estimated to be about ± 10%.

TABLE 2 CALCULATED EVAPORATION VELOCITY FROM THE THREE-DIMENSIONAL BOLTZMANN DISTRIBUTION

Material	Evaporation Temperature (^{0}K)	Mass of Species (g/mole)	Calculated Velocity (10^5 cm/sec)		
			Most Probable	Average	r.m.s.
BN	3273 (subl.)	B^+ = 10.82	2.245	2.533	2.755
Al_2O_3	2523 (b.p.)	Al=26.97	1.250	1.412	1.534
Soda-Lime Glass	1278 (working)	Ca^+=40.08	0.728	0.823	0.894

The most probable, the average, and the root-mean-square velocities are given by $(2kT/M)^{1/2}$, $(8kT/\pi M)^{1/2}$, $(3kT/M)^{1/2}$, respectively.

exceeding 2×10^7 watts/cm^2 in the early part of the pulse, the laser energy is strongly absorbed by the LSD wavefront (Ref. 1) and the target-coupling is greatly reduced. This is evident for the 15-joule cases in which the species arrival time at 1 mm is later than it is for the low energy cases.

These experimental results lead to the conclusion that thermal processes dominate laser-induced evaporation. However, the vapor is further heated by the laser to above 10^4 ^{o} K where the ionic species become predominant. Thus, there appears to be a non-equipartition of energy between the translational and the electronic degrees of freedom. It is interesting to note that the electron emission from laser-heated metal surfaces in vacuum at a comparable power density is also of a thermal character (Ref. 15).

2. TIME DEPENDENCE OF TWO EMISSION LINES

Experiments with the Boeing double-pulse CO_2 laser system have included the application of an electronic attachment (Hilger-Watts E751) of the quartz prism spectrograph (Hilger-Watts E498) for time-resolved spectroscopy. Preliminary measurements on the temporal behavior of several emission lines from the laser-produced plasma have been made.

For time-resolved experiments, the advantages of using the present setup compared with the combination of a transmission spectrograph (TRW 42A) and an image converter camera (TRW 1D described in Section III.1 are: (a) extended wavelength coverage to the near uv, and (b) improved spectral resolution. In brief, a movable narrow slit (width 0.4 mm) was positioned at the image plane of the quartz prism spectrograph. Photons within a small energy spread were detected by a photomultiplier (EMIG255B) which was sensitive in the near uv to visible range. The wavelength versus slit-position calibrations have been made with reference lamps of mercury, helium, and hydrogen, and an electric discharge containing copper. A total of about 100 well-established emission lines were used for the range from 2000 Å to 7000 Å. The signal output was either measured with an electrometer or displayed on an oscilloscope (Tektronix 549, storage type) for photographic recording.

In this experiment, the double-pulse CO_2 laser was used and two 15 joule pulses with a pulse separation of approximately 50 μsec were produced. Two LSD waves were generated with a mirror (of focal length f = 37.5 cm) to focus both laser beams at near normal incidence onto the same area of a target surface. The spectrograph was positioned at 90^{o} to the laser beams and looked at a narrow slice of space 2 mm in front of the target. Figure 5 shows typical oscilloscope traces from three emitting species of the plasma generated from an aluminum plate by two laser pulses. The data were obtained from three separate shots; however, the laser performance was quite reproducible.

The following conclusions may be drawn from the results shown in figure 5.

(1) The second pulse evaporates more aluminum than does the first one.

(2) Atomic aluminum travels at a slower speed compared with the laser-supported absorption wave, which contains mainly N^{+} and O^{+}.

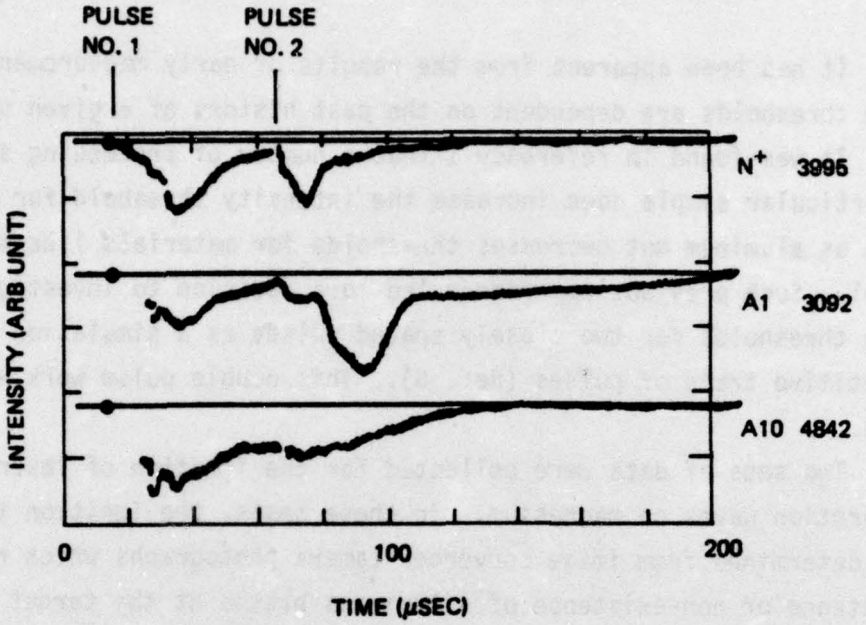


Figure 5. Temporal Behavior of Emission Lines From the Plasma Produced By Two 15-Joule Pulses Separated by 50 μSec. The Spectrograph Is Looking at 2mm in Front of the Aluminum Target

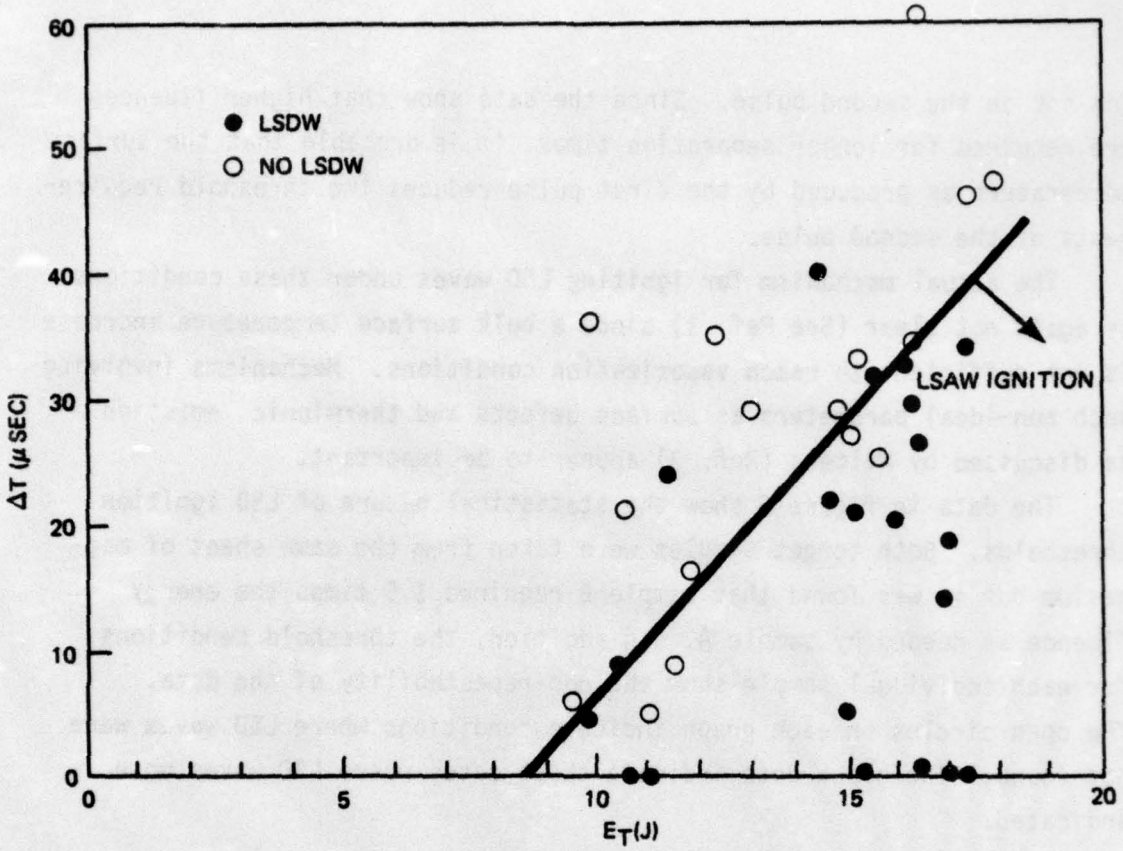
SECTION IV

DOUBLE PULSE LSA WAVE IGNITION THRESHOLDS ON MAGNESIUM

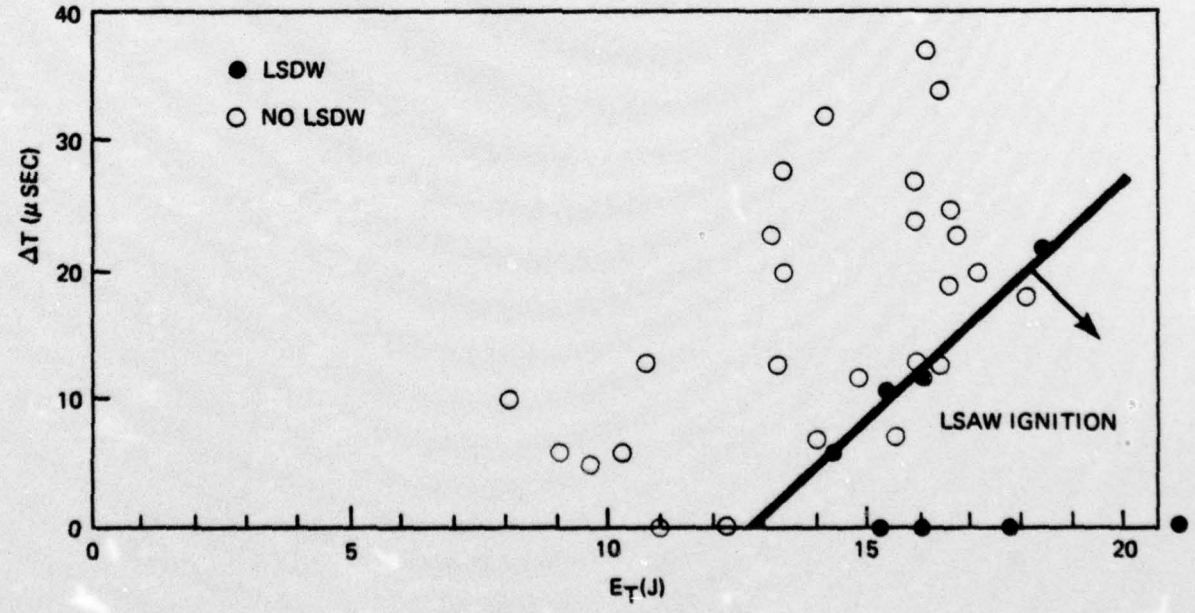
It has been apparent from the results of early measurements that LSA wave thresholds are dependent on the past history of a given sample (Ref. 1). It was found in reference 1 that a number of preceeding shots on a particular sample does increase the intensity threshold for materials such as aluminum but decreases thresholds for materials like stainless steel. Such previous experience led to a decision to investigate LSA wave thresholds for two closely spaced pulses as a simulation of a repetitive train of pulses (Ref. 6). This double pulse work was extended here.

Two sets of data were collected for the ignition of laser-supported absorption waves on magnesium. In these tests, the ignition threshold was determined from image converter camera photographs which recorded the existence or non-existence of a luminous plasma at the target surface during the laser pulses. The time between the two separate laser pulses was varied electronically, although system jitter did not allow absolute control. This separation time and the energy in the laser beams was measured in each test. Laser beam energy was varied by plastic attenuators common to both beams and laser operating conditions were not varied.

Figures 6a and 6b show test results obtained with two different magnesium targets each of which absorbed a large number of laser pulses. The two sets of data (samples A and B corresponding to figures 6a and 6b respectively) indicate the dependence of the total laser energy E_t to ignite LSD waves as a function of the interpulse separation time Δt. The energy E_t is the sum of the energies in both pulses (it varied between 8 and 21 joules in these experiments) required to ignite an LSD wave on the second pulse of the double-pulse sequence. In each case, both the first and second pulse had nearly equal energies. The two sets of data clearly indicate that a thermal threshold is important in igniting these LSD waves. If the laser intensity were the only parameter of importance, LSD waves would have always been ignited on the first pulse



A. Magnesium Sample A



B. Magnesium Sample B

Figure 6. Plasma Ignition

and not on the second pulse. Since the data show that higher fluences are required for longer separation times, it is probable that the surface temperature as produced by the first pulse reduces the threshold requirements of the second pulse.

The actual mechanism for igniting LSD waves under these conditions is again not clear (See Ref. 1) since a bulk surface temperature increase is not sufficient to reach vaporization conditions. Mechanisms involving such non-ideal parameters as surface defects and thermionic emission as discussed by Walters (Ref. 3) appear to be important.

The data in figure 6 show the statistical nature of LSD ignition thresholds. Both target samples were taken from the same sheet of magnesium but it was found that sample B required 1.5 times the energy fluence as needed by sample A. In addition, the threshold conditions for each individual sample show the non-repeatability of the data. The open circles on each graph indicate conditions where LSD waves were not found. The black dots indicate those cases where LSD waves were indicated.

SECTION V

IMPULSE ON TARGETS AND AIR PRESSURE PULSES PRODUCED BY DOUBLE-PULSE CO_2 LASER RADIATION

The experiments reported in this section were all designed to determine if the impulse produced by two temporally close laser pulses can produce more impulse than two pulses separated by a long time. The initial logic for this expectation was discussed in reference 5 where it was shown that the blast wave produced by the first of two laser pulses can increase the LSD wave threshold for the second pulses because of the decreased gas density near the target surface. Under these conditions, one would expect more surface vaporization from a metal under double-pulse conditions than for a single pulse of equal or greater total energy. In reference 5 the impulse was measured for lead as a function of pulse separation and an optimum pulse separation of approximately 50 μsec was found. However, the same type data was also measured by Lincoln Laboratories with aluminum targets and no significant impulse enhancement was found (Ref. 16). Because of these discrepancies a new series of experiments were undertaken.

Three metals were used in the impulse tests: 6061 aluminum, 304 stainless steel, and titanium. All were used in the as-received condition, except for a cleaning with methyl alcohol to remove organic contaminants. These materials were prepared in the form of disks of diameter 1.59 cm, 1.27 cm, 0.95 cm, and 0.79 cm. The aluminum disks were 0.112 cm thick, the stainless steel disks were 0.068 cm thick, and the titanium disks were 0.094 cm thick. All the disks were mounted with tape on the moving element of the Trans-Tek Model Number 100-000 linear velocity transducer (LVT). The mass of the moving element, adaptor, tape, and all the various target material-size combinations were measured to within (± 5 mg) or about ± 0.1% of the total moving mass. About 80 to 90% of the moving mass was the LVT core. The LVT and moving core element were calibrated with tests which used a mechanical spring pusher which was constrained to deliver an impulse during the first 0.05 cm of motion by

a stop and which allowed 0.600 ± 0.10 cm of free motion before the moving element assembly bottomed out in the LVT housing. The calibration of velocity versus voltage agreed with the manufacturer's estimate.

The laser focal spots for these double-pulse CO_2 tests were superimposed and were 0.70 ± 0.02 cm diameter. Two 80 cm focal length mirrors were used to focus the beams. (This arrangement almost duplicated the spot size of the focused HF laser beam when it was focused by a 37.5 cm focal length mirror, see Vol. I.)

Output signals from the LVT are produced during the motion of the moving core assembly; however, all of the data reported here are for the peak signals which occurred within a few milliseconds. Total motion lasted for 10 or more milliseconds and the LVT output signals were recorded on a Tektronix 549 oscilloscope.

With this long focal length, the ignition thresholds for laser-supported absorption waves were not always reached and in those instances no measurable impulse was produced. This ocurred both for the titanium tests when the interpulse separation was more than 10 microseconds and also for stainless steel. The laser fluence needed at 10.6 μ for titanium LSD wave ignition was previously found (Ref. 17) for a 0.244 cm diameter spot to be about 160 J/cm^2. For the above spot size, however, only one plasma ignition was observed.

The impulse data for aluminum are shown in figure 7 as a plot of impulse/incident energy versus the pulse separation time. Each of the four target sizes has been used and a wide variety of interpulse separation times are shown. It can be seen from these data that synchronized laser pulses (shown at Δt = 1 μsec) produce a larger ratio I/E than do the separated pulses. In general, the ratio I/E decreases both as the interpulse separation time is increased and as the target diameter is decreased. This behavior occurs for double pulses because the surface pressures produced by the second LSD wave are reduced. The decrease in impulse for smaller targets occurs, as described by Pirri (Ref. 18), because the expanding blast waves have less surface area to act over.

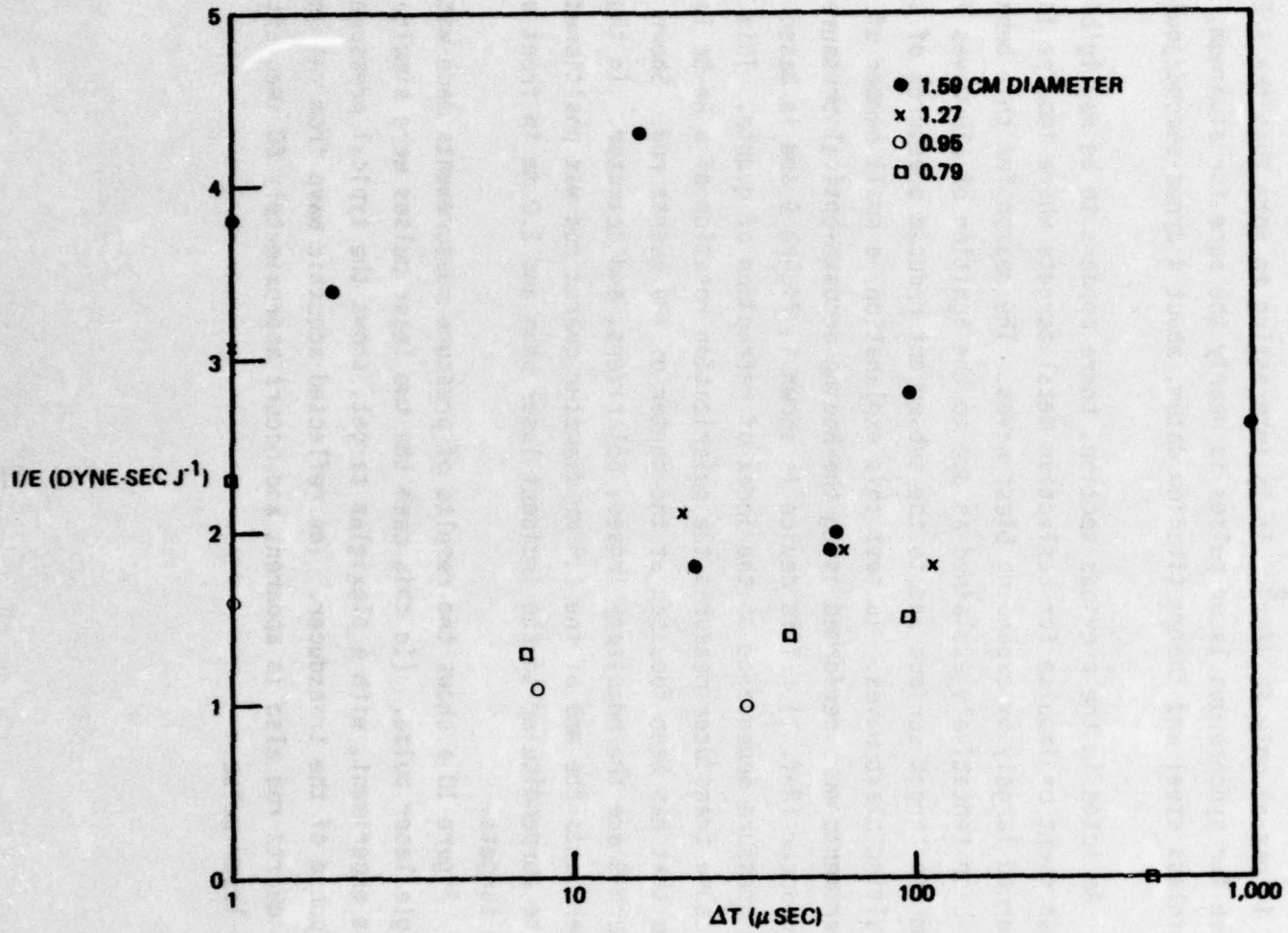


Figure 7. I/E Values Shown as a Function of Separation Time for Aluminum

When 304 stainless steel targets were used, data were difficult to obtain because the plasma ignition threshold was exceeded only on some of the shots due to the large spot size and the slight variability of the laser pulse energy. The data that were collected are shown in figure 8. The single datum point with the large uncertainty value was retrieved from an off-scale oscillograph trace and does not represent typical uncertainties.

The data obtained for titanium included only one plasma ignition and it was at only 42 J/cm^2. It is interesting to note that the I/E value for synchronous laser pulses is nearly the same for aluminum, 304 stainless steel and the one titanium datum, about 4 dynes-second/joule.

As noted in the previous section, there appears to be negligible enhancement of impulse for reflective metal targets where impulse is governed largely by expanding blast waves. The reason for this behavior has been tentatively explained as due to the ignition of LSD waves further from the target surface and to the subsequent reduced pressures of the resulting blast waves. To test this explanation, a small number of experiments was performed using the Boeing acousto-optical pressure transducer (Ref. 1). This device is shown in figure 9 and is based on the pressure dependence of the index of refraction of quartz. This pressure transducer measures the polarization rotation of a He-Ne laser beam that has been focussed at the center of the quartz rod. Shown in figure 9 are the necessary lenses, polarizers, and detector. In these experiments the end of the 1.5 mm diameter quartz rod was positioned to be perpendicular to the incident laser beam and 2.0 mm in front of the targets.

Figure 10 a shows the results of pressure measurements made with a single laser pulse. (In this case the two laser pulses were simultaneous.) This experiment, with a plexiglas target, shows the typical pressure response of the transducer. The reflected acoustic wave from the end of the quartz rod also is apparent and occurs approximately 60 μsec after the laser pulse.

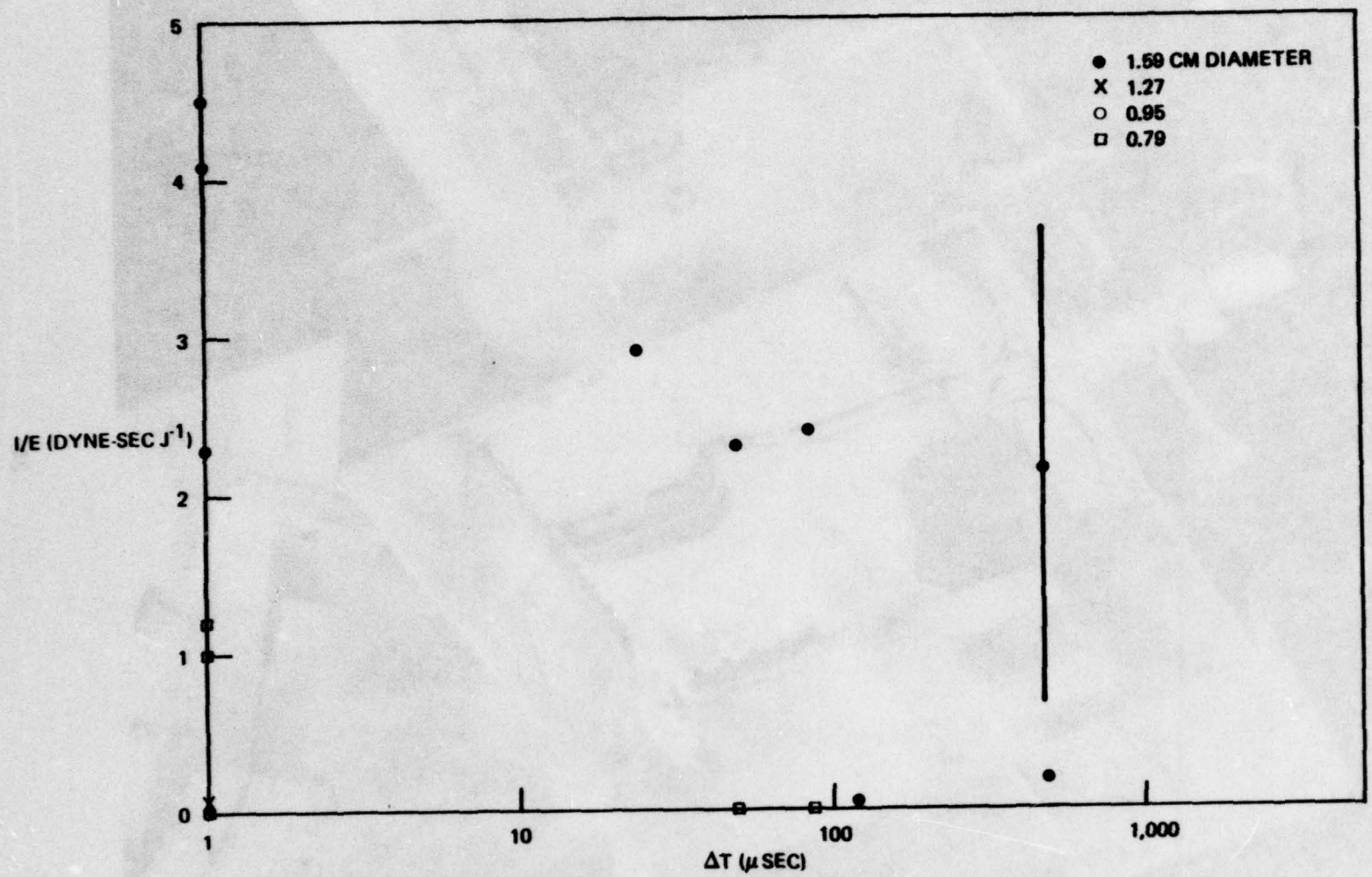


Figure 8. I/E Values Shown as a Function of Separation Time for 304 Stainless Steel

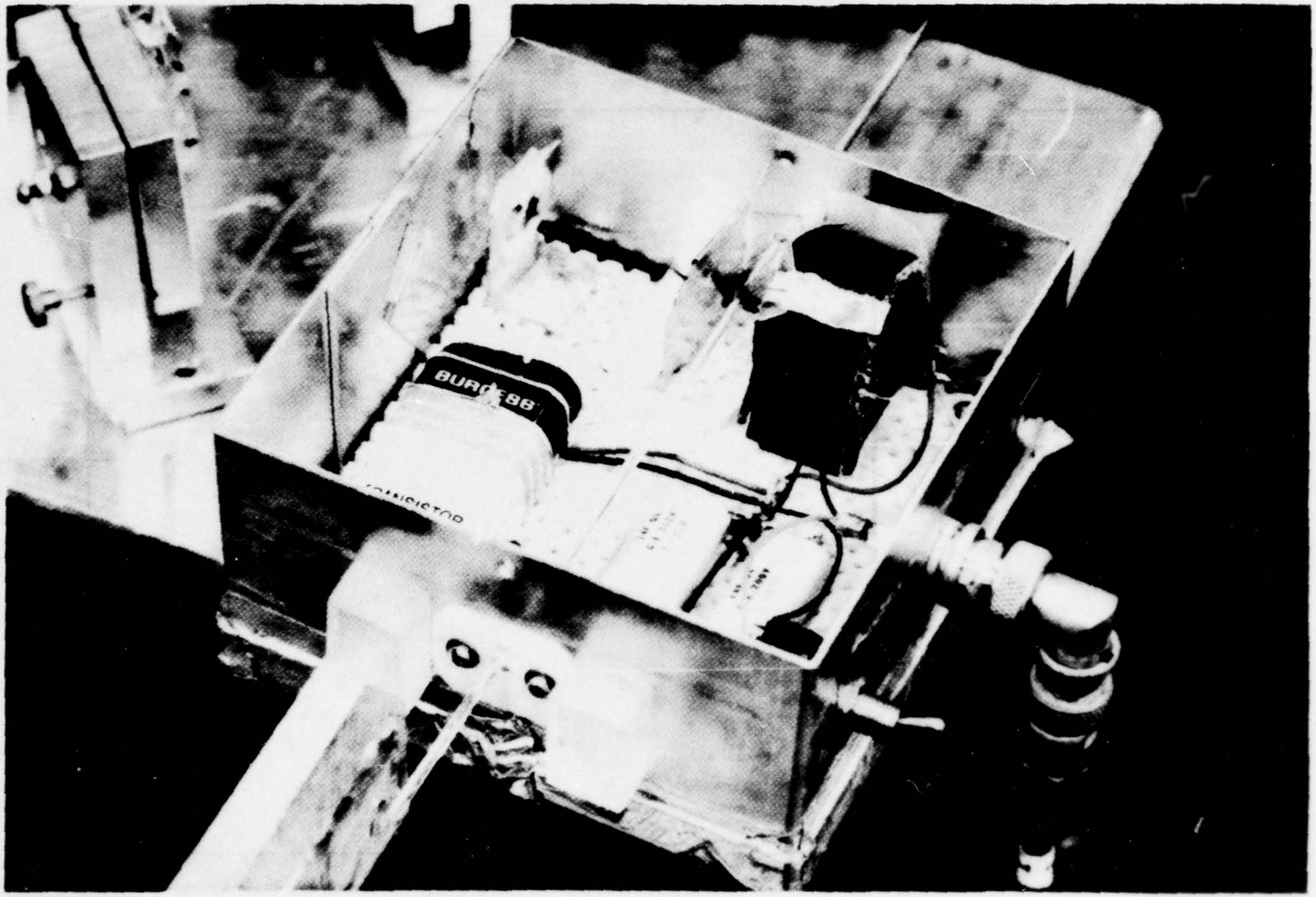


Figure 9. Boeing Pressure Transducer

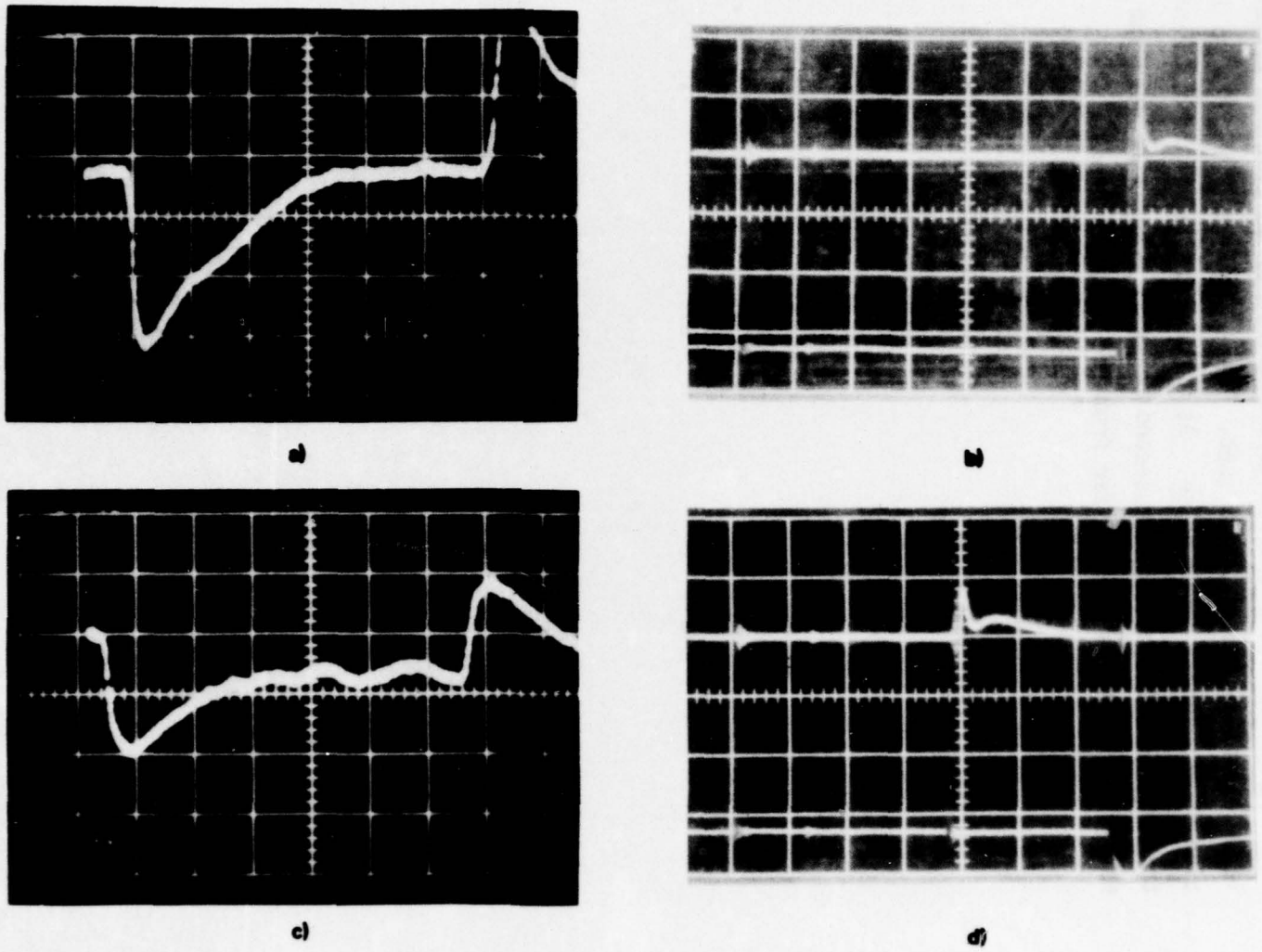


Figure 10. Pressure Transducer Measurements (10 μsec/Division)
a) Lucite Target Pressure Pulses b) Incident Laser Pulses for (a),
c) Aluminum Target Pressure Pulse, d) Incident Laser Pulses for (c)

Figure 10c shows the pressure response of an aluminum target to laser pulses separated by 26 μsec. These pressure data show no indication of the second laser pulse. As a consequence, it is apparent that the impulse delivered by the second pulse is greatly reduced and that the second LSD wave was ignited far from the target surface.

SECTION VI
THERMAL COUPLING MEASUREMENTS

1. BASIC DATA

Thermal coupling phenomena were previously discussed in Volume I for the HF laser beam-target interaction. The CO_2 laser beam-target interaction is similar with an enhancement appearing above some threshold in fluence or intensity. The intrinsic absorptivity at 10.6 micron of aluminum, however, is only about one third that at the 2.8 micron wavelength. For this reason, thermal enhancement in coupling is particularly important for pulsed CO_2 lasers since a true enhancement in coupling can greatly reduce the total laser power required. In order to understand repetitively pulsed effects, it was decided to first do a sequence of experiments with a single pulse at a wavelength of 10.6 μ. This should provide some insight into the proposed mechanisms of enchanced coupling observed by Rudder and Carlson (Ref. 19) and by Gilbert and Carlson (Ref. 20).

In the first experiments reported here, the laser pulse was focused with a 37.5 cm focal length mirror on a 2024 alloy aluminum disc target having a diameter of 1.59 cm and a thickness of 0.081 cm. Using a mass density of 2.7 and the tabulated heat capacity of aluminum of 0.9 joule/gm/^{o} C, one obtains the total heat capacity of one of these targets to be 0.39 joule/^{o} C. Thus, by measuring the temperature rise of the target, one determines the absorbed energy.

Figure 11 summarizes the results of a first set of experiments. The average coupling (defined as the ratio of the heat absorbed by the target to the energy incident on the target) is nearly constant at a value of $\alpha = 0.023$ for all laser pulses that do not ignite laser-supported absorption (LSA) waves. In general, laser-supported absorption waves (LSA waves) include waves at both supersonic and subsonic speeds, (Ref. 21). At high laser intensities, ($\sim 10^6$ to 10^7 watts/cm^2) LSA waves are usually supersonic and are normally called laser-supported detonation waves, LSD waves.

For a "dirty" target surface, (LSD) waves are ignited for this laser pulse shape for laser energies greater than 7.5 joules. As a consequence of the ignition of these plasmas, one observes a marked increase in the coupling efficiency. The maximum coupling of 0.19 is approximately eight times that observed without plasma production. For laser energies greater than threshold however, one observes a rapid decrease in the coupling coefficient as the incident laser energy is increased. It appears that the coupling efficiency α is proportional to E^{-1} for energies greater than threshold and implies that a constant energy is absorbed at the target.

All the datum points in the figure were taken with a single target starting with the highest available laser energies. The circled datum points labeled "cleaned" target were taken toward the end of this particular sequence and indicate the tendency toward target surface "cleaning" in which LSD waves are not ignited after repeated laser shots on the same focal spot (Ref. 17).

An explanation for the observed cleaning tendency would be the vaporization of small detached surface flakes; however, no detailed study of this phenomenon has been attempted.

Next, a double-pulse test geometry was set up which also allowed tests at reduced pressures. This is shown schematically in figure 12. Both laser beams enter the vacuum chamber through separate KCl windows and inside the chamber are brought to a common focus on the target.

Figure 13 shows the thermal coupling to a magnesium target located in a vacuum chamber with a pressure of 1/100 atmosphere. Each laser shot used a fresh new target so that target history played no role. At this low pressure, the pulse separation time was found to play almost no role, although experiments in the range 1 μsec $< \Delta t <$ 200 μ sec were performed. The total laser energy was the sum of the energy of both the first and second pulse. It should be noted that there were two distinct thresholds dependent on the energy fluence. The first is that lowest fluence where there is a permanent marking of the target surface resulting from vaporization or melting. At this lower threshold no

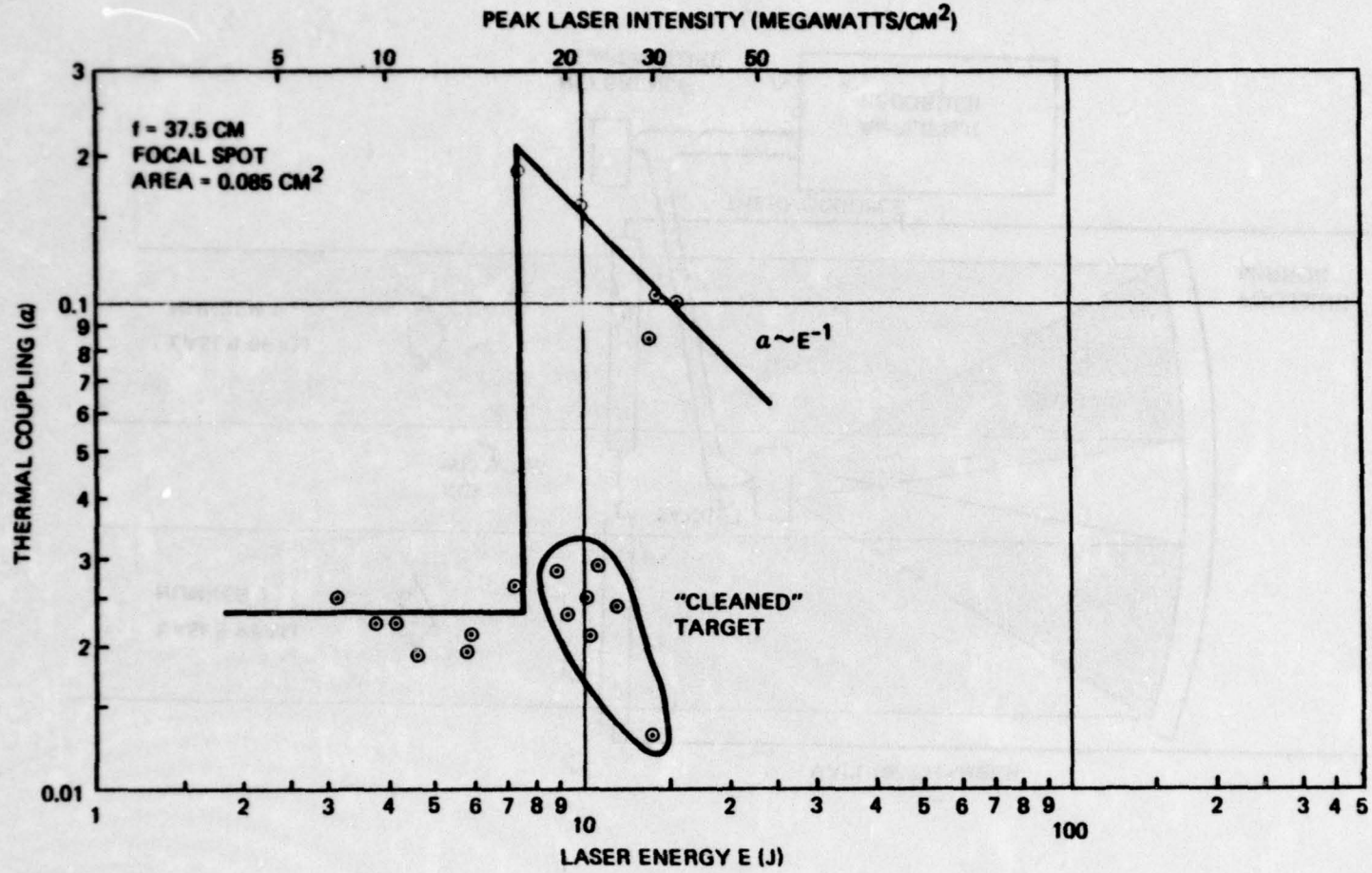


Figure 11. Coupling Efficiency as a Function of Laser Intensity for Single 10.6 Micron Pulses

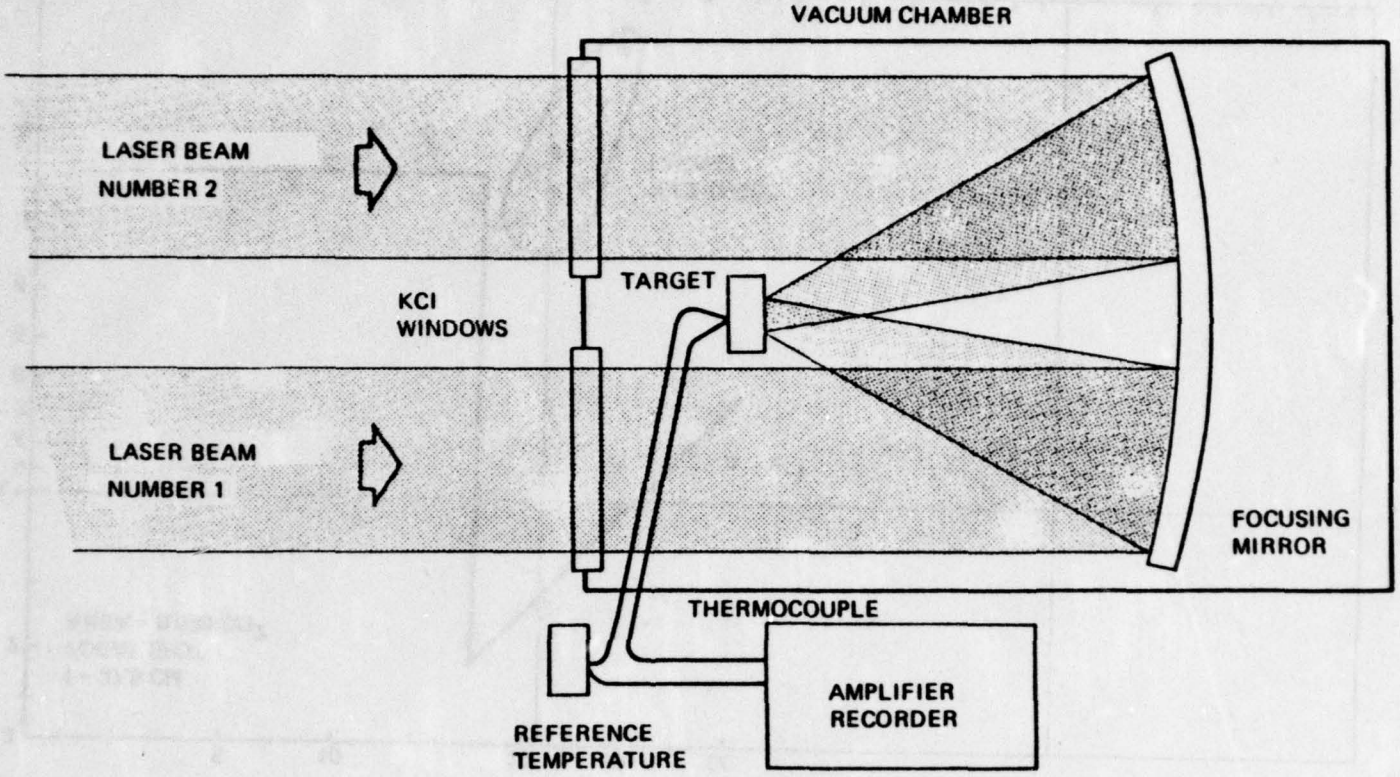


Figure 12. The Experimental Apparatus for Double Pulse Thermal Coupling

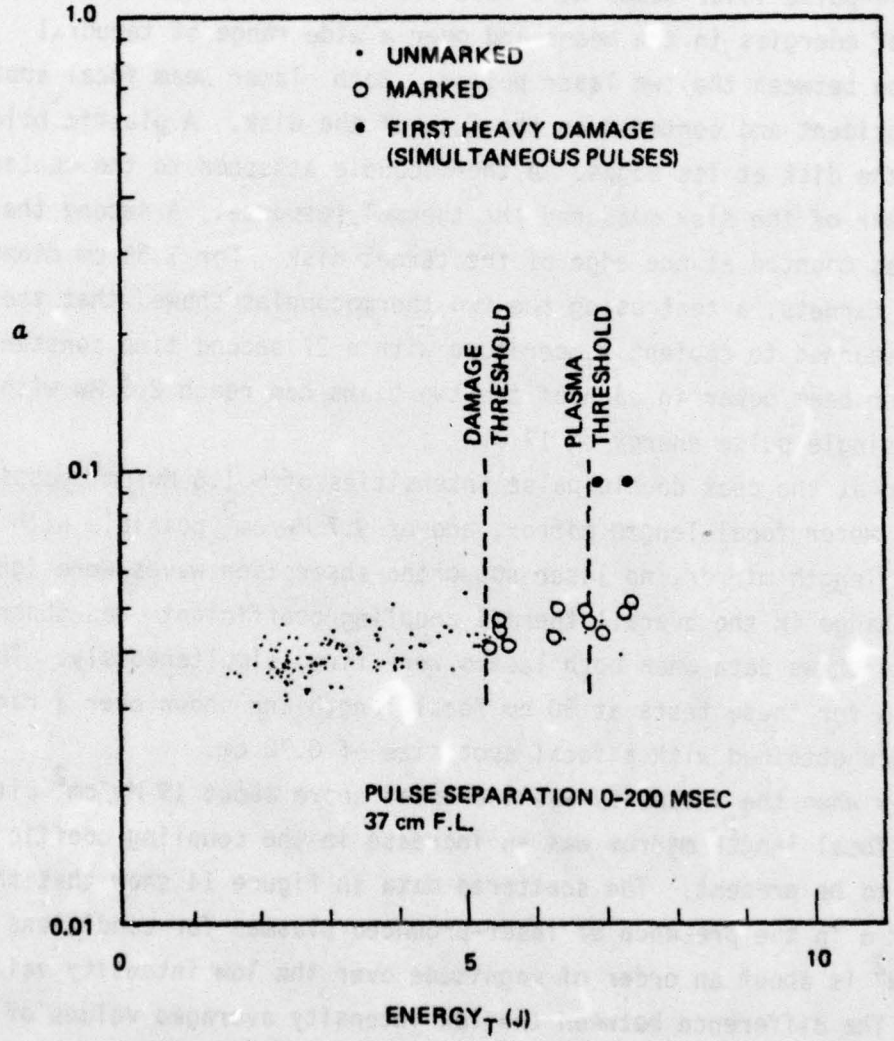


Figure 13. Double Laser Pulse Thermal Coupling to Magnesium at 1/100 Atmosphere at and Below Plasma Threshold

surface plasma was produced as observed with an image converter camera. At the higher threshold, a plasma plume was produced and more heavily cratered surface damage was observed. Under these conditions, a jump of nearly a factor of two in the measured thermal coupling α occurred.

2. SPOT SIZE DEPENDENCE

Measurements of the thermal response of aluminum disk targets to the double-pulse laser beams were made for three focal spot sizes with a range of energies in the beams and over a wide range of temporal separation between the two laser pulses. Both laser beam focal spots were coincident and centered on the face of the disk. A plastic holder clamped the disk at its edges. A thermocouple attached to the center of the rear of the disk measured the thermal response. A second thermocouple was mounted at the edge of the target disk. For 1.59 cm diameter aluminum targets, a test using the two thermocouples showed that the target returned to ambient temperature with a 27 second time constant. Peak laser beam power in each of the two beams can reach 2.5 Mw with the maximum single pulse energy of 17 J.

Even at the peak double-pulse intensities of $\sim$ 1.6 Mw/cm^2 possible with a 2 meter focal length mirror, and of 9.7 Mw/cm^2 possible with a 80 cm focal length mirror, no laser supported absorption waves were ignited and no change in the overall thermal coupling coefficient was observed. Figure 14 shows data when both lasers were fired simultaneously. The average α for these tests at 80 cm focal length are shown over a range of fluence obtained with a focal spot size of 0.70 cm.

Only when the intensity was increased above about 19 Mw/cm^2 with a 37.5 cm focal length mirror was an increase in the coupling coefficient, α, seen to be present. The scattered data in figure 14 show that the value of α in the presence of laser-produced plasmas for conditions above 19 Mw/cm^2 is about an order of magnitude over the low intensity value of 0.028. The difference between the low intensity averaged values of α obtained for the two mirror focal lengths of 37.5 cm and 80 cm is comparable to the 25% data scatter found in these experiments. In this experiment the absolute uncertainty in E_t is $\pm$13%, but the relative uncertainty in the E_t measurements is only about $\pm$ 2%. The absolute undertainty in

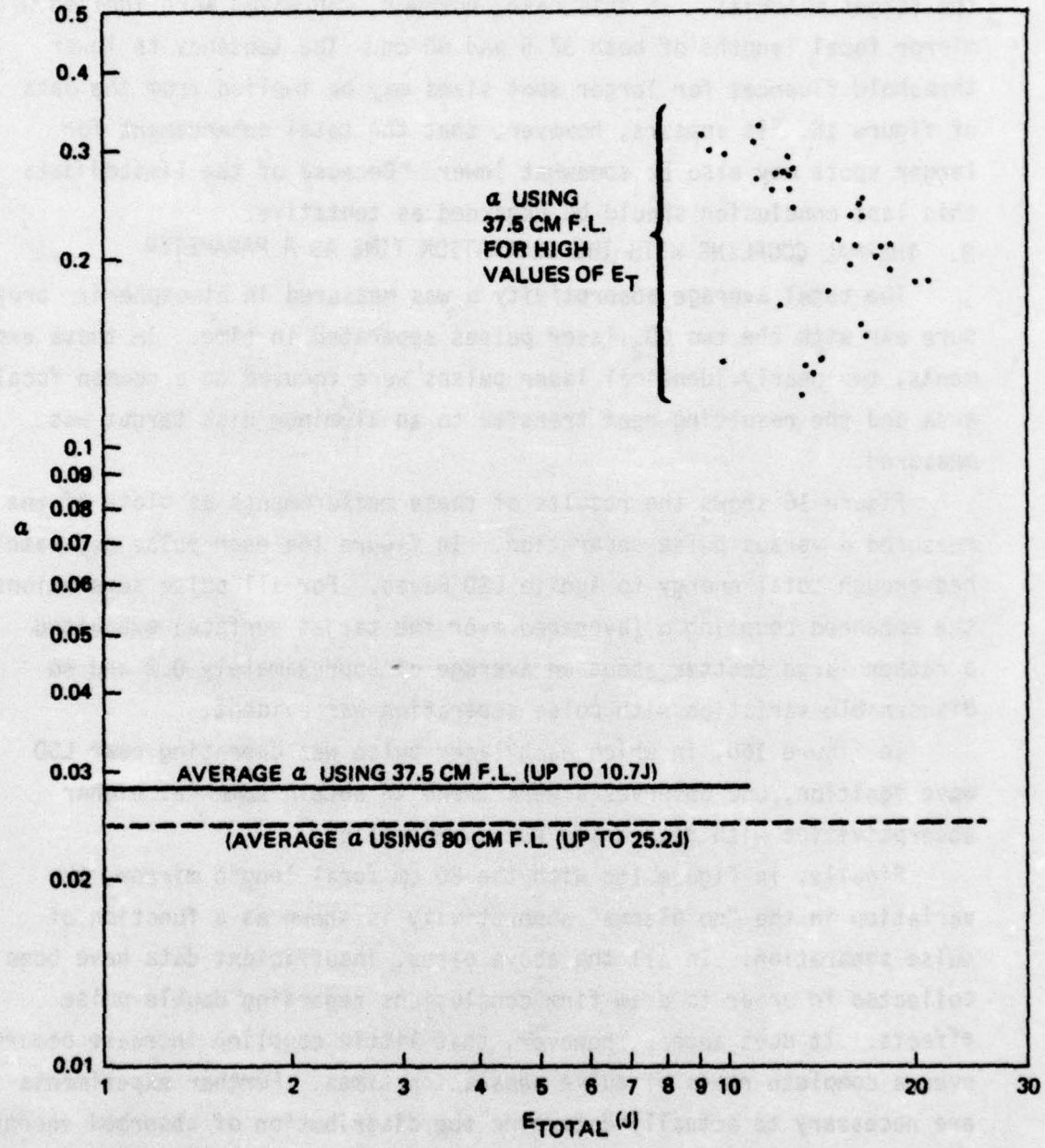


Figure 14. Aluminum Absorption Coefficient Enhancement

the values for α is $\pm$ 14%.

A similar set of experiments was carried out using magnesium as the target material. In this case, however, LSD waves were ignited with mirror focal lengths of both 37.5 and 80 cm. The tendency to lower threshold fluences for larger spot sizes may be implied from the data of figure 15. It appears, however, that the total enhancement for larger spots may also be somewhat lower. Because of the limited data this last conclusion should be regarded as tentative.

3. THERMAL COUPLING WITH THE SEPARATION TIME AS A PARAMETER

The total average absorptivity α was measured in atmospheric pressure air with the two CO_2 laser pulses separated in time. In these experiments, two nearly identical laser pulses were focused to a common focal area and the resulting heat transfer to an aluminum disk target was measured.

Figure 16 shows the results of these measurements as plots of the measured α versus pulse separation. In figure 16a each pulse separately had enough total energy to ignite LSD waves. For all pulse separations, the enhanced coupling α (averaged over the target surface) exhibited a rather large scatter about an average of approximately 0.2 and no discernable variation with pulse separation was evident.

In Figure 16b, in which each laser pulse was operating near LSD wave ignition, one observes a weak trend to obtain somewhat higher absorptivities with decreasing pulse separation.

Finally, in figure 16c with the 80 cm focal length mirror, the variation in the "no plasma" absorptivity is shown as a function of pulse separation. In all the above cases, insufficient data have been collected in order to draw firm conclusions regarding double-pulse effects. It does appear, however, that little coupling increase occurs over a complete range of pulse separation times. Further experiments are necessary to actually determine the distribution of absorbed energy on the target surface under double-pulse conditions. It is possible that the energy density may tend to be more concentrated toward the center of the focal spot with a double-pulse than with single high intensity laser pulse.

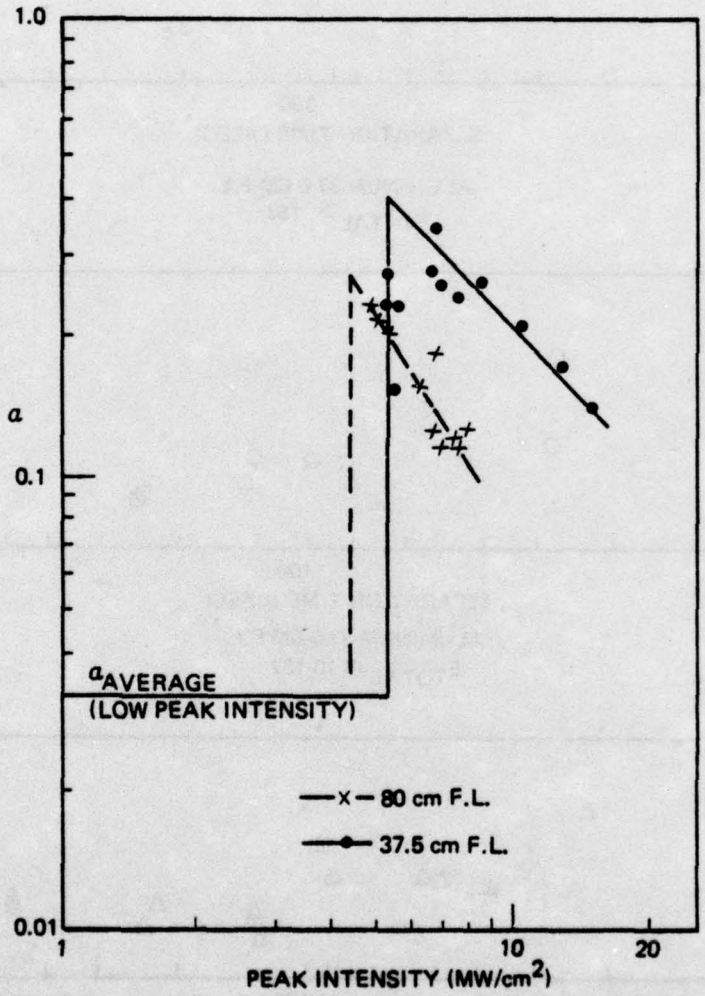


Figure 15. Thermal Coupling to Magnesium at One Atmosphere for Two Spot Sizes

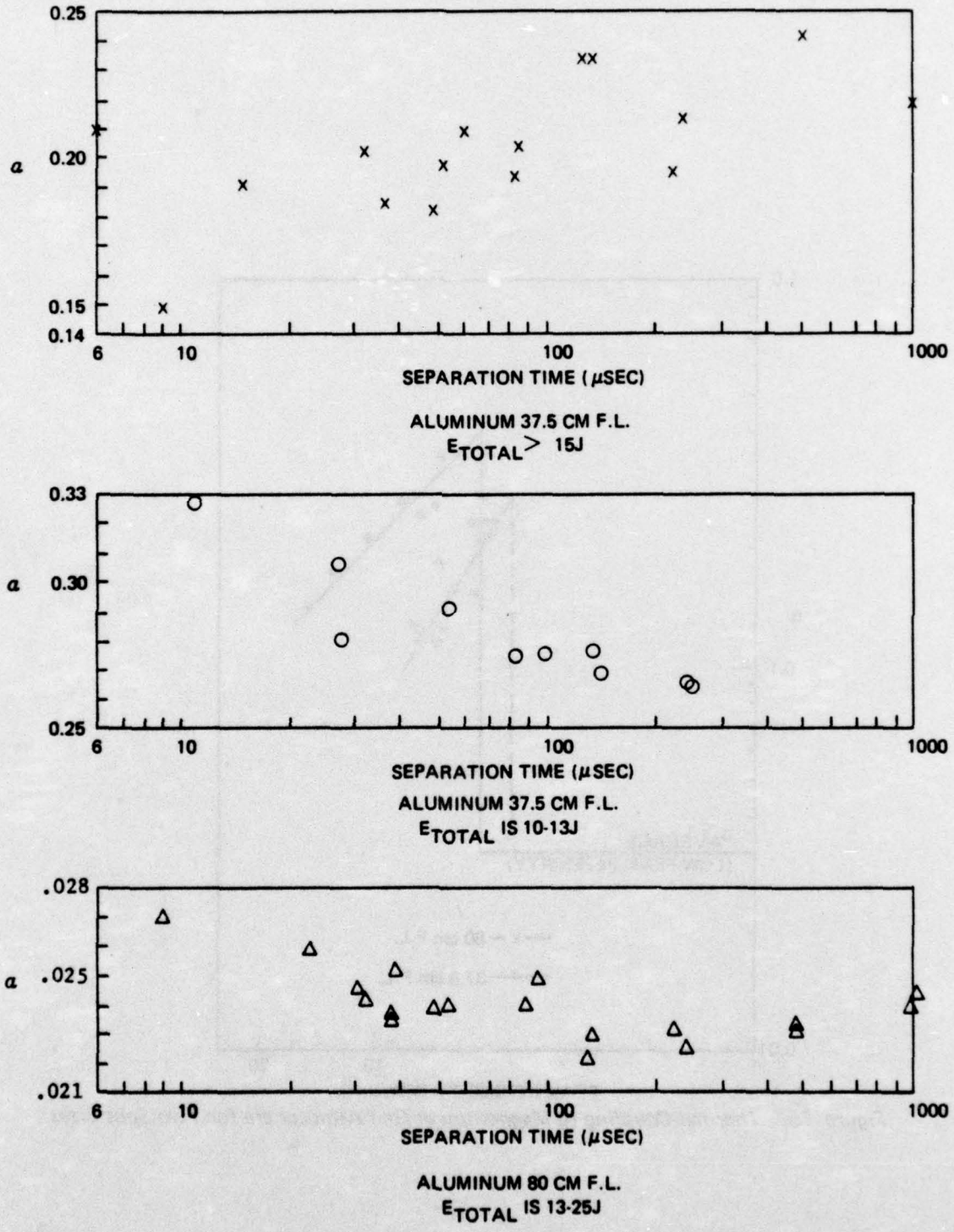


Figure 16. Sensitivity of Absorption Coefficient to the Separation Time

As mentioned above, very little evidence was seen of any strong sensitivity of these thermal coupling processes to the double-pulse separation time. This is again evident in the magnesium target data shown in figure 17. These data taken at 1/100 atmosphere indicate the similarity between the enhancement of thermal coupling produced by single pulses and that produced by nonsimultaneous pulses. The thermal coupling coefficient is plotted against the total incident energy. When the pulses are separated by 200 microseconds, the thermal coupling is lower for low energies and rises more slowly, but eventually rises above that obtained for simultaneous pulses.

The experimental data with magnesium targets indicate that the second pulse of a double-pulse train couples somewhat less thermal energy to targets than a single equivalent energy pulse. This is seen in figure 18 where two pulses with separations of approximately 10 μsec couple less energy to the target than occurs with nearly simultaneous pulses. Apparently, the surface temperature created by two separated laser pulses ($\sim$ 10 microseconds) is not adequate to cause vaporization of the surface. This is presumably due to the absorption of laser energy of the second laser pulse in the plasma created by the first laser pulse.

4. PRESSURE DEPENDENCE

The previous measurements at atmospheric pressure were augmented by experiments in the large vacuum chamber shown in figure 2. Equivalent single-pulse laser thermal coupling was measured in the 1 meter diameter vacuum chamber which was fitted with two 10 cm diameter NaCl windows through which the two laser beams enter. All focusing optics and target mounting X-Y mounts were inside the chamber. The term "equivalent single-pulse laser thermal coupling" here means coupling measured with either one pulse or with two simultaneous pulses focused on the same spot.

Figure 19 shows the results of measurements with aluminum targets at pressures of 760, 76 and 2.3 Torr. Only one laser beam was used for the aluminum coupling tests. In the data of figure 19, the open datum points indicated by either Δ (at 0.1 atmosphere) or $\square$ (at 0.003

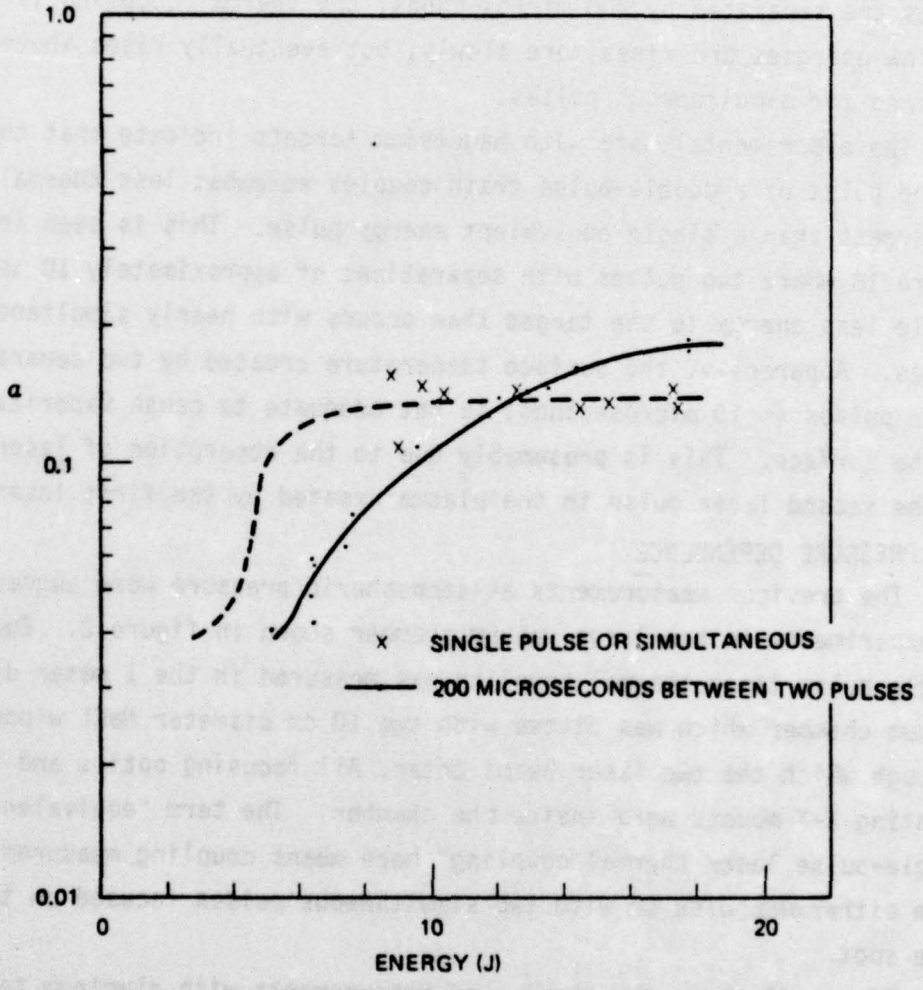


Figure 17. Double Laser Pulse Thermal Coupling to Magnesium at 1/100 Atmosphere

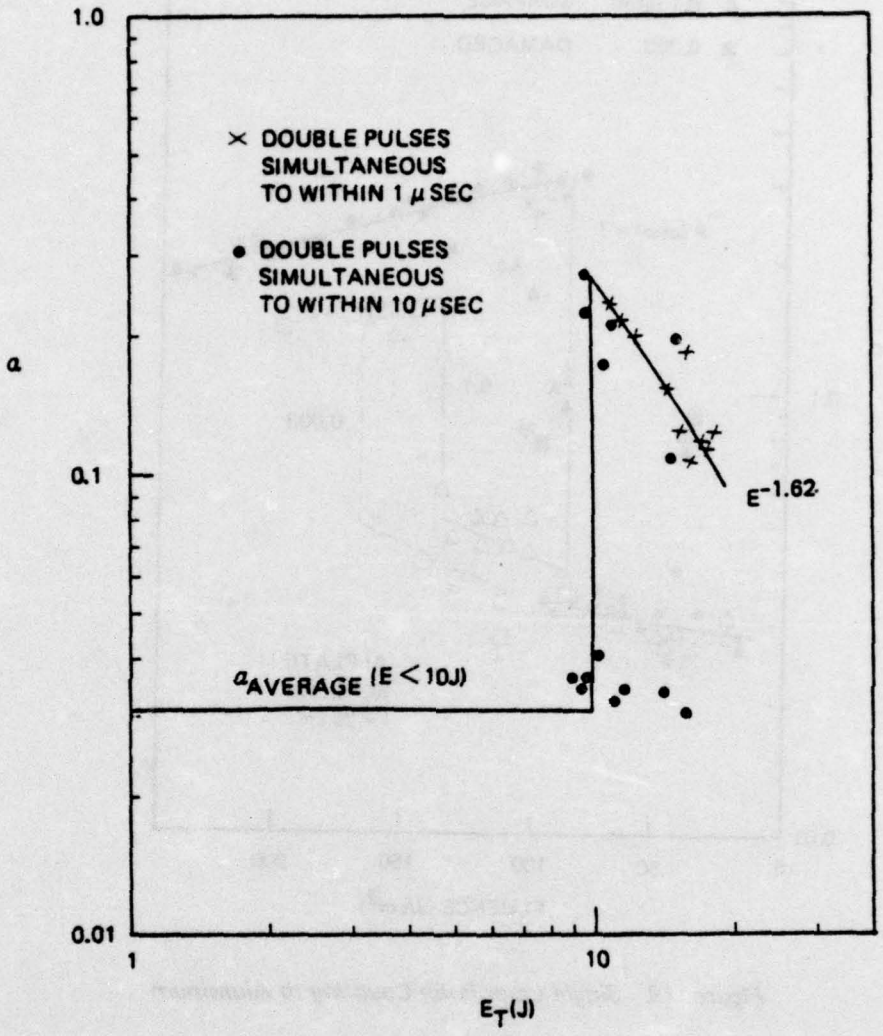


Figure 18. Laser Beam Thermal Coupling to Magnesium: Single and Simultaneous Double Pulses at 80 cm F.L. and One Atmosphere

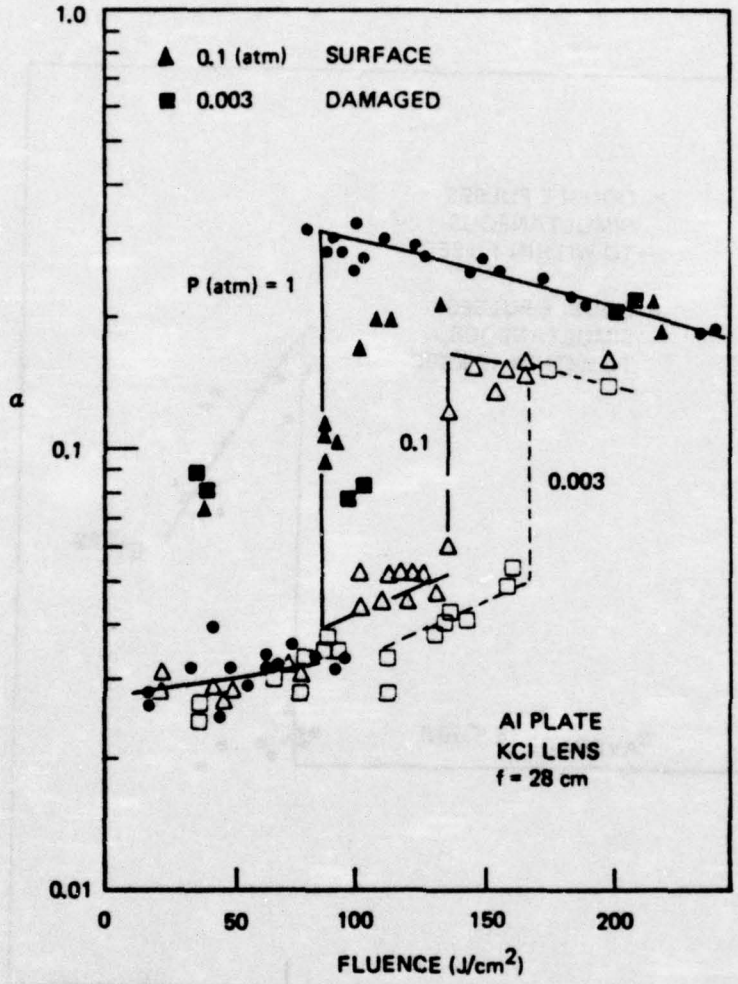


Figure 19. Single Laser Pulse Coupling to Aluminum

atmosphere) indicates that undamaged targets were used in the measurements. At these low pressures, however, the targets were cratered (damaged) after each shot. When these previously damaged materials were used as laser targets the measured thermal coupling was found to be somewhat higher. Thermal coupling data for these "damaged targets" are indicated by either ▲ or ■ for pressures of 0.1 and 0.003 atmospheres respectively.

In these low pressure measurements, the aluminum targets were heavily damaged as is shown in figure 20. This scanning electron micrograph shows the target area damaged at 76 Torr by a total of 10 laser shots. The diameter of the steeply sloped walls of the crater was found to be 2.3 mm with an average depth of approximately 1 mm. This diameter correlates well with the laser focal diameter of 2.44 mm obtained with the 28 cm focal length lens. Since the damaged area in these low pressure experiments was obviously confined to the beam diameter, there does not seem to be the same physical process producing the crater as the process which delivers heat to the target. The radial profile for enhanced thermal coupling is wider than the laser beam focal spot, as is discussed in Section VI.6 below. At these lower pressures the enhancement of thermal coupling was less than at 1 atmosphere but the target damage was much larger.

The pressure dependence of the thermal coupling coefficient was also obtained for both magnesium and stainless steel with a focussing mirror of 37.5 cm focal length. For magnesium, as shown in figure 21, it was found that the threshold for plasma enhancement was independent of pressure below 0.1 atmospheres. It should be noted that the solid data points in figure 21 indicate no previously damaged target surface. The absolute error in the fluence values is believed to be ± 18%, while the absolute errors in α are ± 14%. This compares with about a ± 15% scatter in the subthreshold α values. Figure 22 shows the thermal coupling variation for stainless steel targets. In this case an abrupt threshold was found only at pressures higher than 0.1 atmosphere. There apparently is only a smoothly increasing coupling with increasing fluence for low pressures.

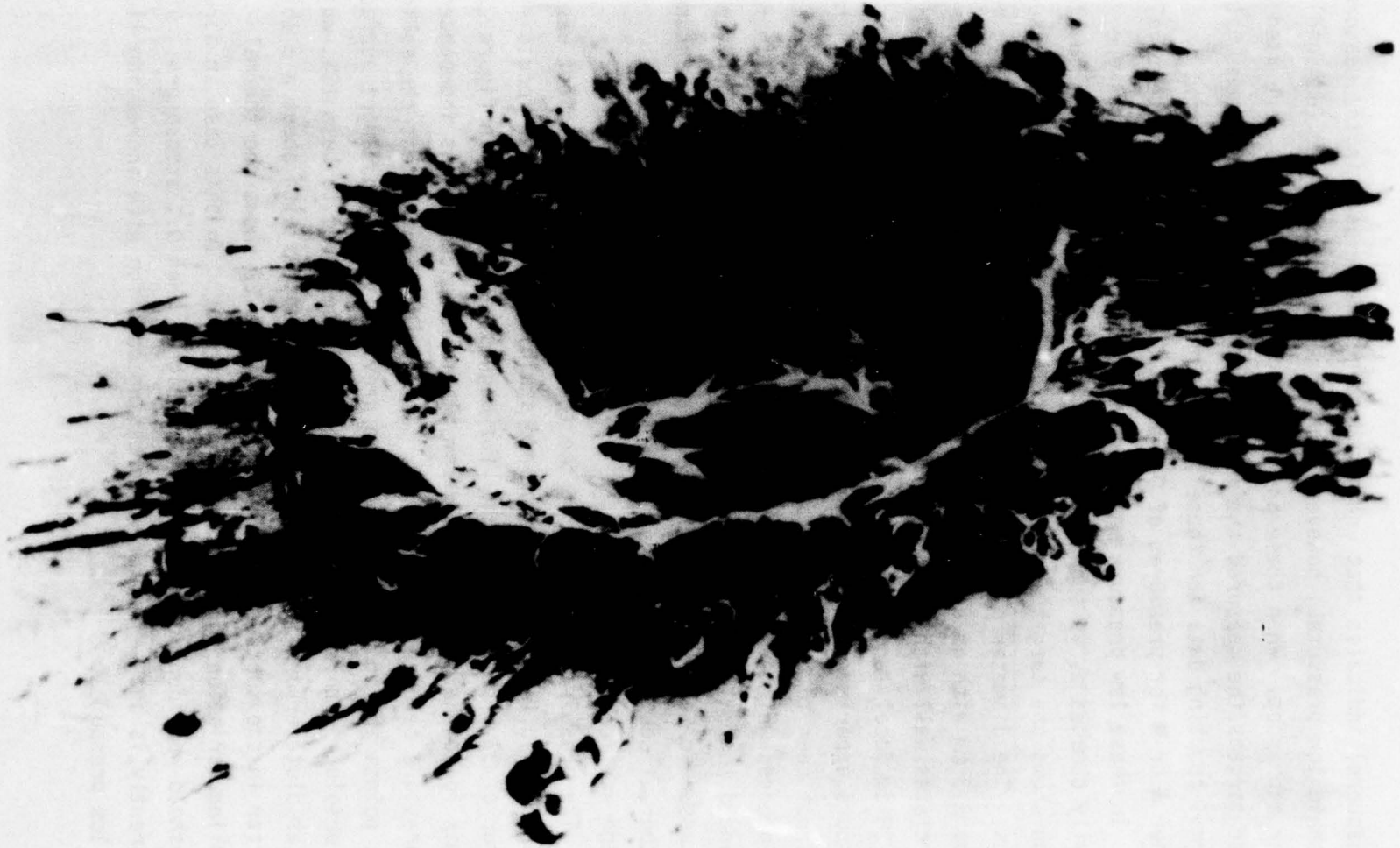


Figure 20. Aluminum Crater Produced at Low Atmospheric Pressure

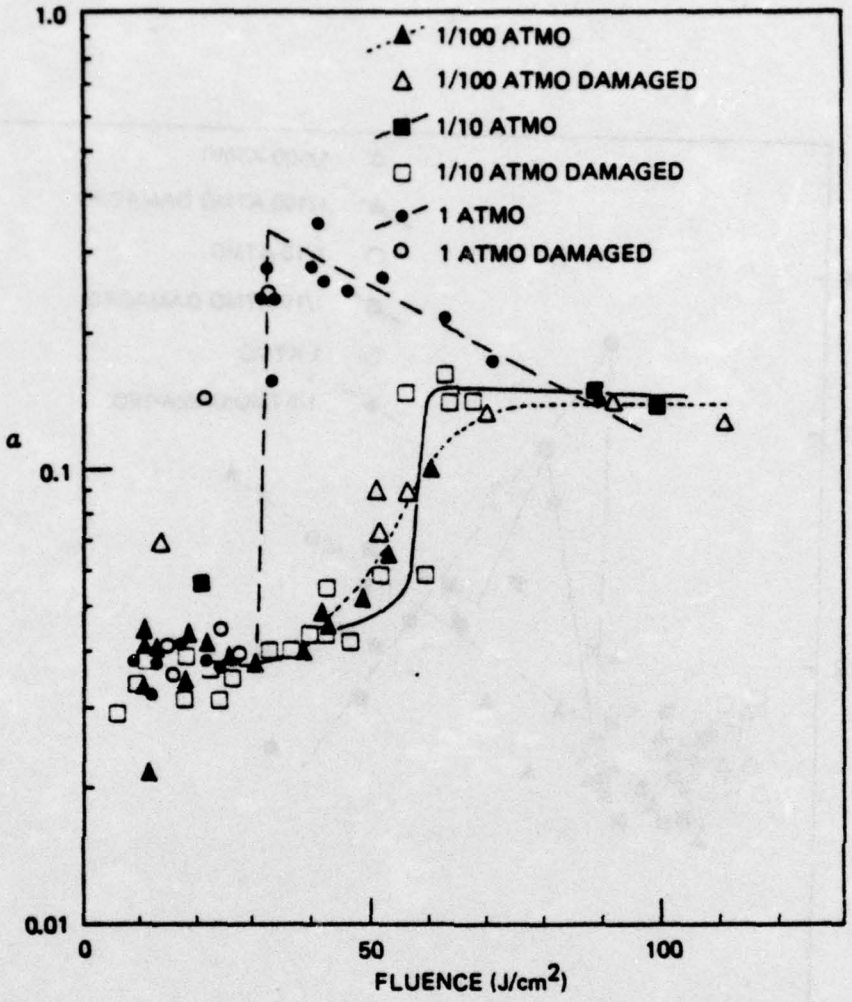


Figure 21. Single Laser Pulse Thermal Coupling to Magnesium

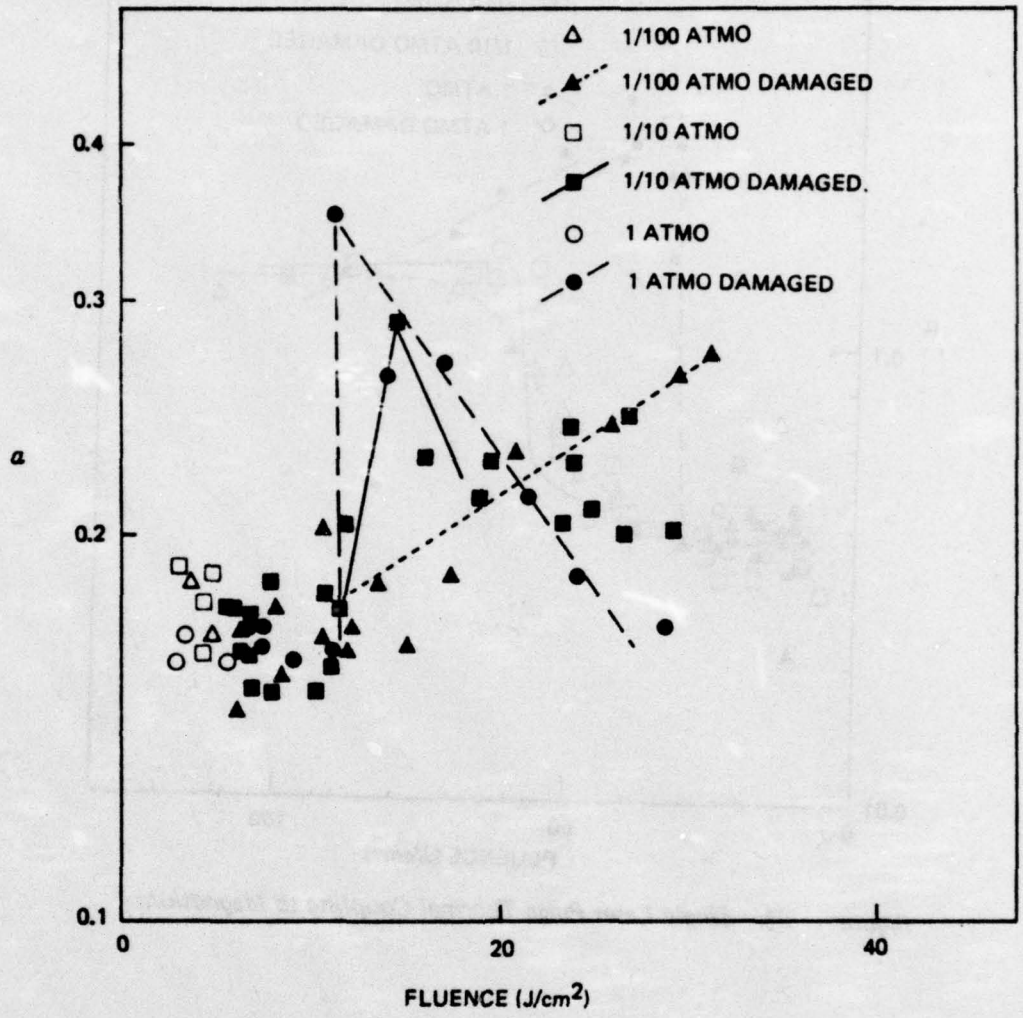


Figure 22. Single Laser Pulse Thermal Coupling to 304 Stainless Steel

5. Spatial Distribution of Absorbed Energy

The above measurements were based on a calorimetric technique in which the total energy absorbed by a target was measured. This was based on a measurement of the equilibrium target temperature and absolutely no information was obtained about the distribution, over the target surface, of the absorbed energy. It was crucial, however, to determine where on the target surface the absorbed energy was actually deposited. This is important since low intensity heating over a large area is not effective in damaging targets even though large total energies may be transferred. In figure 13, for example, target damage was shown to occur at lower fluences than required for plasma ignition. Figure 20, on the other hand, showed that accumulated target damage in aluminum occurred at low pressures only in the focal spot area.

In order to determine the deposited energy density profile (in joules/cm^2) delivered to a target under "enhanced coupling" conditions several experiments were tried. One preliminary experiment included attempts to vary the effective exposed target diameter by the insertion of circular apertures in front of the target surface. These aperture sizes varied from the outer target diameter down to a diameter slightly larger than the focal spot diameter and were placed concentric with the beam and 1 mm in front of the target. The concept being examined was the possibility that much of the additional energy transferred to the target during enhanced thermal coupling was delivered to the area lying well outside the laser beam focal spot. When the data were taken and evaluated, no clearcut dependence of the absorption coefficient on the aperture diameter could be found. Probably hot gases and evaporated material were able to move into the space between an aperture and the target, and, as a result, the apertures did not shield the target surface. It was clear, however, from these initial experiments that energy was transferred to radii considerably larger than the focal radius. As a result, a reliable measurement technique which would not perturb the plasma was sought.

It is evident that sufficiently thin targets could have been used to determine the deposited energy density profile on the front surface. This would be possible, for example, by measuring the back surface temperature with many thermocouples as a function of radius. Thus, if the thermal energy has not diffused significantly in the radial direction when temperature measurements are made, one could hope to determine the profile of deposited energy. One problem of this technique is that many matched thermocouples would have to be carefully attached to the target.

The technique actually adopted was based on the classical expression for the temperature response of a solid to a constant, axially symmetric energy deposition. Since thick metal targets obviously do not receive a constant deposition of laser power along the axis of the laser beam, one may not expect such an expression to be of value. If one is not interested in the actual details of the intensity (watts/cm^2) as a function of time, however, one can determine the energy density profile as a function of radius. This is made possible by utilizing a thermally thin target. In such a target, the axial heat diffusion time is less than any radial heat diffusion times. For such targets and for times greater than the actual laser pulse width, the above requirements of an axially uniform deposition of energy are satisfied.

The time response of the thin-target temperature is given by Ready, (Ref. 22) at arbitrary radii and times. It is interesting to note, however, that the back surface (or front surface) temperature, at r = 0, for circularly symmetric energy deposition is given by

$$T(t) = \frac{1}{4DKt} \int_0^\infty e(r^2) e^{\frac{-r^2}{4\kappa t}} dr^2 \qquad (3)$$

where D = target thickness (cm)

t = time

K = thermal conductivity (watts/cm/K)

κ = thermal diffusivity (cm^2/sec)

e = energy density ($joules/cm^2$)

r = radius (cm)

Thus, one sees from Equation 3 that the temperature as a function of time as observed at r = 0 is a modified Laplace transform of the energy density profile. In principle then, one can uniquely determine the exact energy profile of absorbed energy by measuring the time-dependent temperature at r = 0 and performing an inverse Laplace transform.

The requirement of a thermally thin target means that the temperature (or energy density) profile does not spread significantly in the radial direction during the time in which the temperature is equilibrated in the axial direction. For purposes of analysis, the laser pulse emitted by the Boeing Marx bank laser for this series of measurements can be approximated by the temporal shape shown in figure 23. For times greater than about 14 microseconds, the laser power falls to zero with a straight-line slope. The measured energy density profile at the focus of a lens (or mirror) is given approximately by equation 1. Because of the short laser pulse, the heat diffusion equation is essentially one-dimensional. The partial differential equation determining temperature in a slab is (assuming temperature-independent thermal properties),

$$\left.\begin{aligned} \frac{1}{\kappa}\frac{\partial T}{\partial t} &= \frac{\partial^2 T}{\partial z^2} \\ -\kappa \left.\frac{\partial T}{\partial z}\right|_{z=0} &= q(t) \text{ watts/cm}^2 \\ \left.\frac{\partial T}{\partial z}\right|_{z=0} &= 0 \end{aligned}\right\} \qquad (4)$$

In equation (4), the laser intensity q is given by

$$q(t) = p(t)\left(\frac{E}{11} \times 10^6\right) \text{ watts/cm}^2 \qquad (5)$$

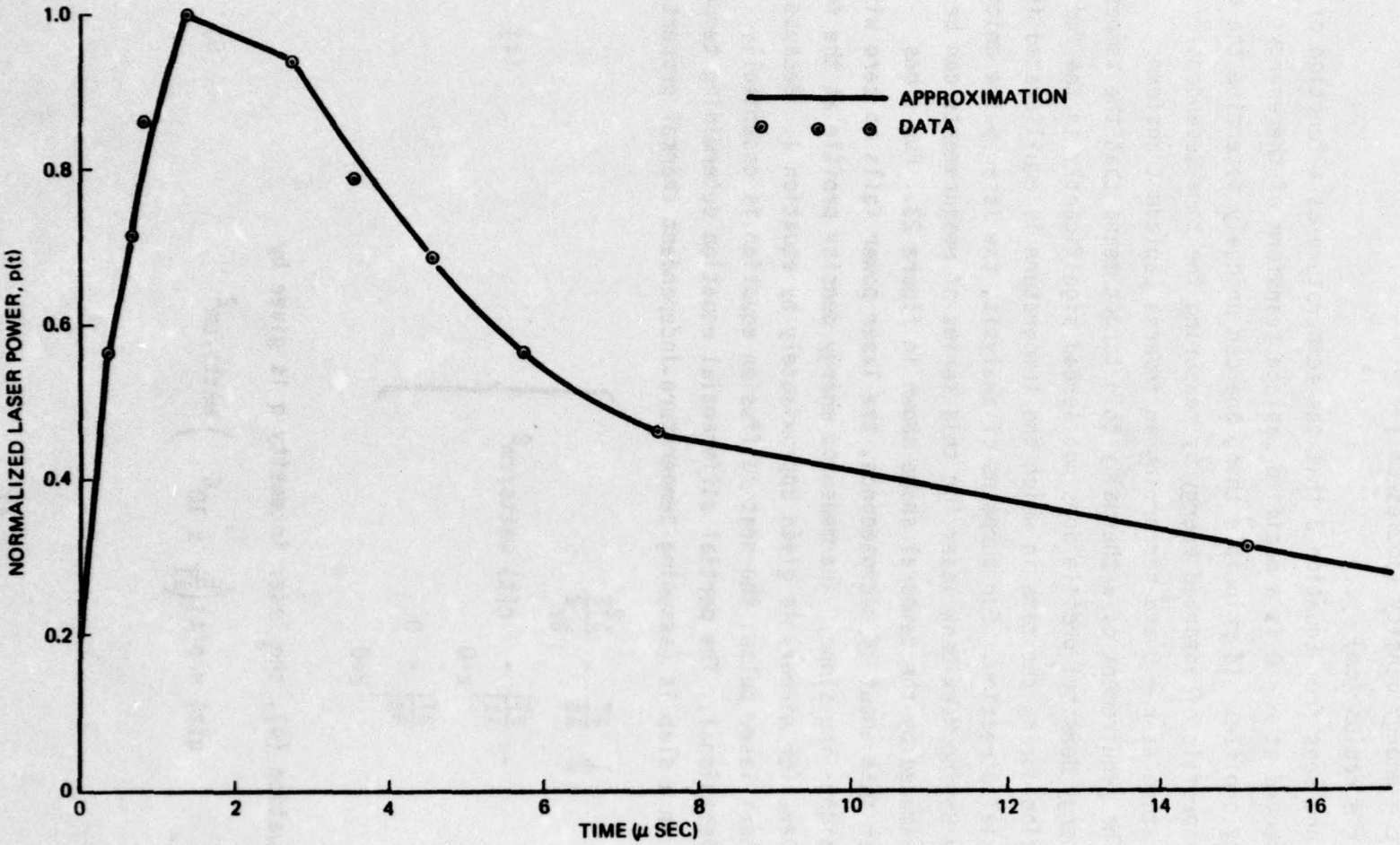


Figure 23. Laser Power as a Function of Time

where p(t) is shown in figure 23.

When the above laser pulse is incident on a finite thickness metal slab, the surface temperature rises quickly and then decays and reaches the final equilibrium temperature of the slab. For an aluminum slab with

α = 0.023 = absorptivity
K = 2.16 watts/cm/K
C = 2.51 joules/cm^2/K (6)
D = target thickness = 0.028 cm
E = incident laser energy = 1.68 joules

the front and rear surface temperatures were determined by solution of equation 4 and are shown in figures 24 and 25. For this laser energy, the maximum surface temperature increase is 120^{o}K. It should be noted, however, that this thermal problem is linear and that all temperature increases are linear with the incident laser energy. This indicates that a target which is initially at room temperature (293^o K) will reach the melting point of Al (at 933^o K) with an incident laser energy of 8.9 joules. From figure 25, the equilibration time (defined as the time when both front and back temperatures are within 10% of the final temperature) is seen to be approximately 300 microseconds. The actual temperature distribution within the slab itself is shown in figures 26 and 27 for an incident energy of 2 joules. (It should be recalled that figures 24 and 25 are plotted for E = 1.67 joules.) Thus, for comparison with figures 26 and 27 all temperatures on figures 24 and 25 should be multiplied by 1.2).

Since the temperature is nearly completely equilibrated throughout the target slab thickness by a time of $\sim$ 0.3 μsec, the concept of a diffusion time, τ_d, appears valid.

$$\tau_d = \frac{D^2}{4\kappa} \text{ sec} \qquad (7)$$

where
D = thickness (cm)

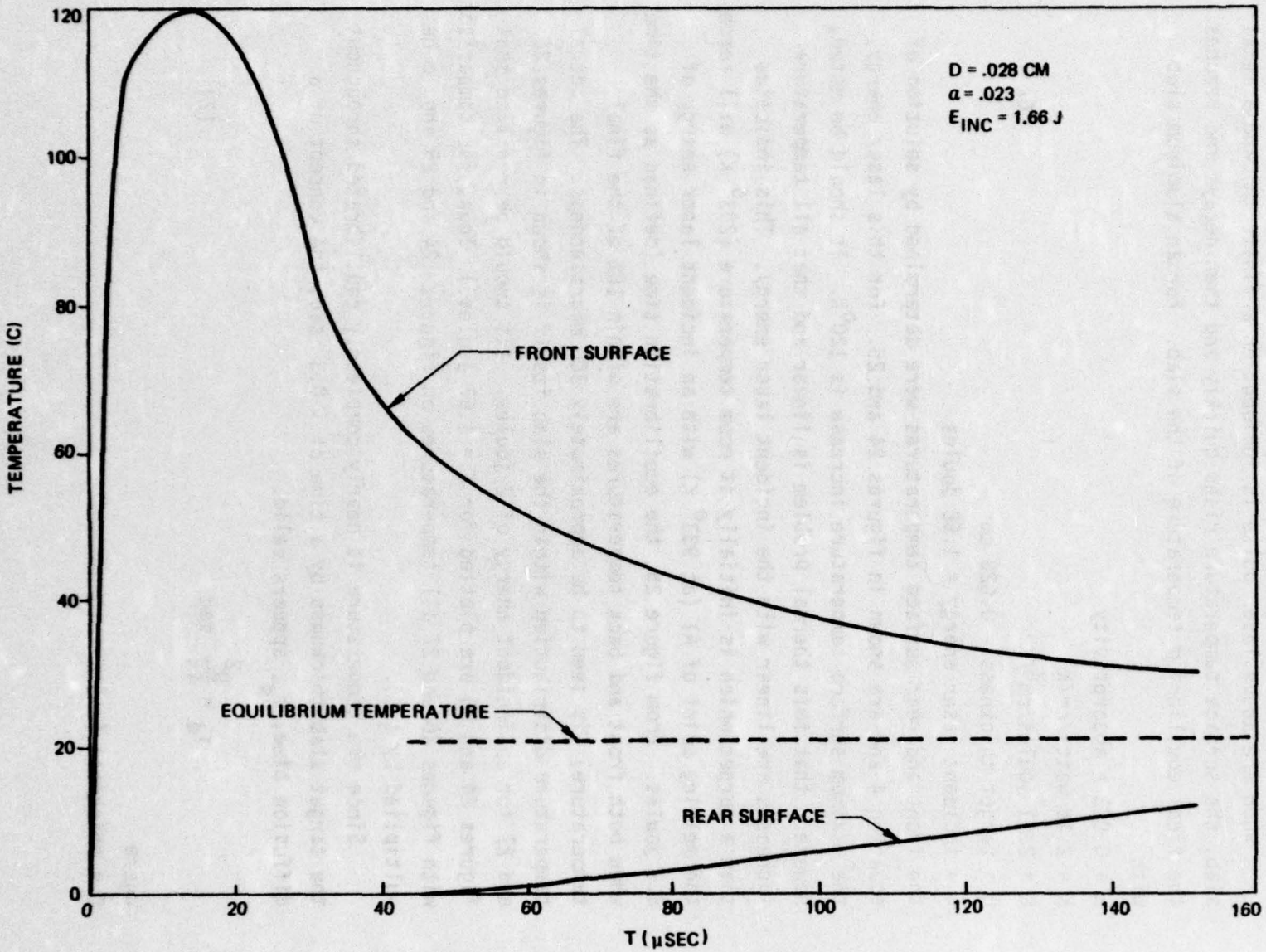


Figure 24. Front and Rear Surface Temperature Time Dependence

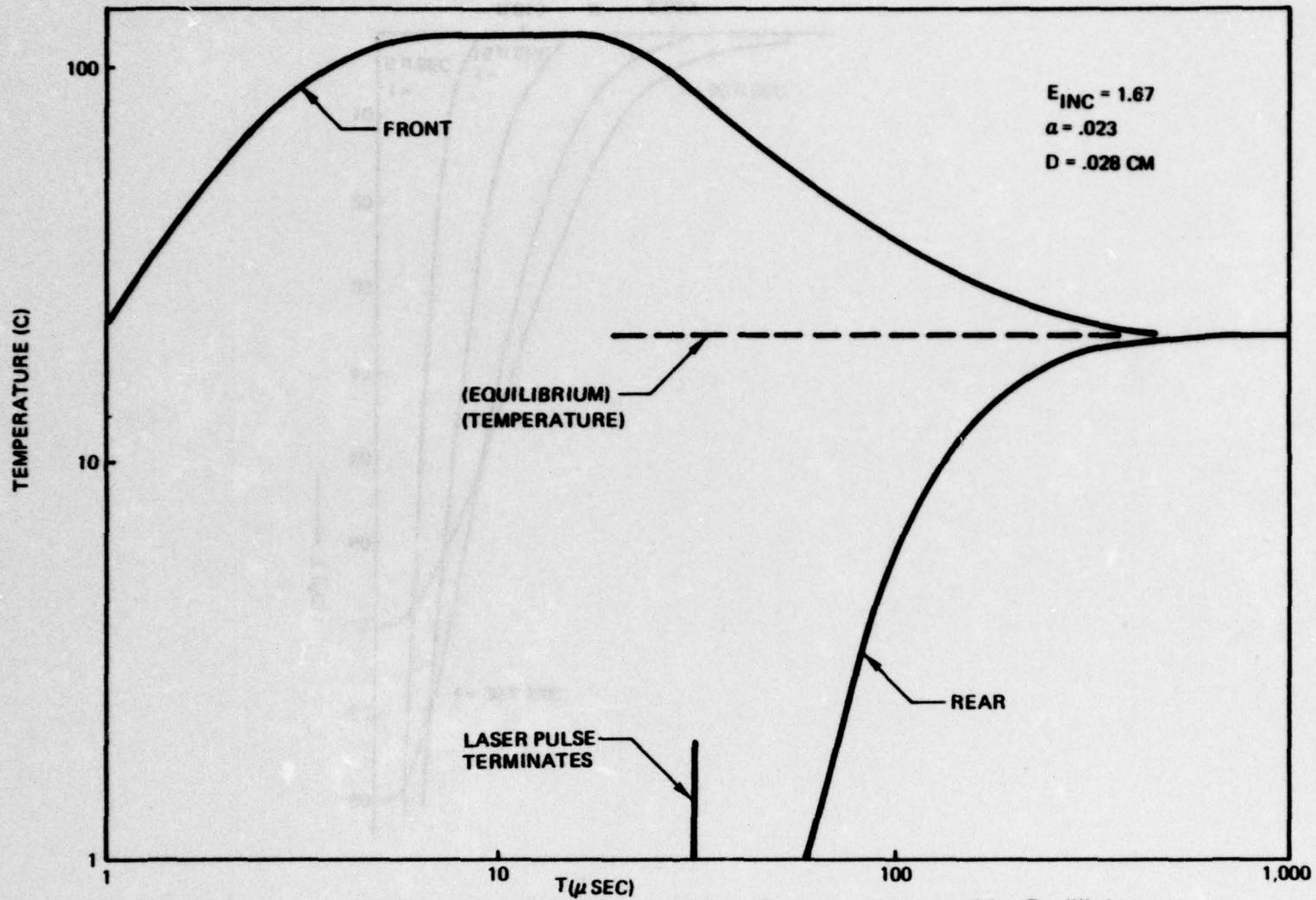


Figure 25. Logarithmic Plot of Front and Rear Temperature Approaching Equilibrium

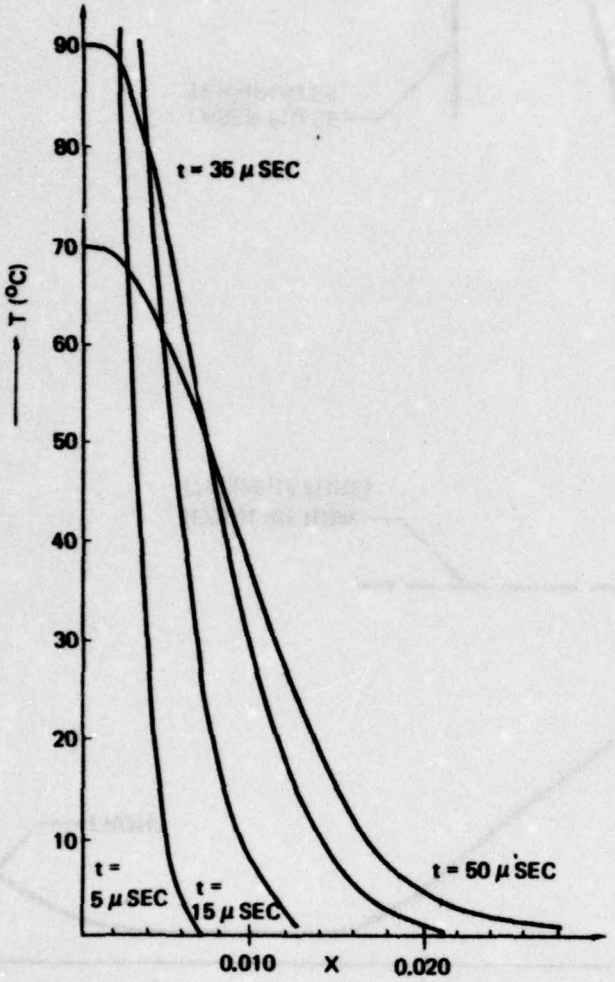


Figure 26. Temperature Profile in an Aluminum Sheet 0.028 cm Thickness. Laser Pulse Energy was 2 Joules in a Spot 2.5 mm Diameter and With a Surface Absorptivity of 0.023.

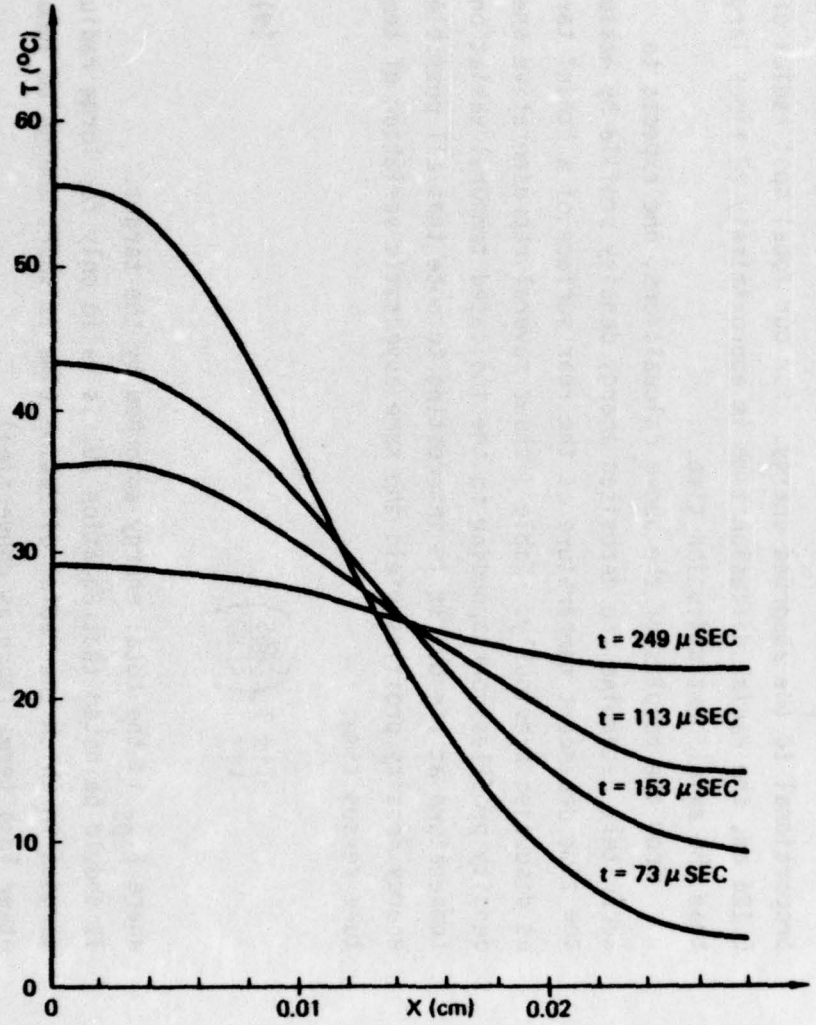


Figure 27. Temperature Profile in an Aluminum Sheet 0.028 cm Thickness. Laser Pulse Energy Was 2 Joules in a Spot 2.5 mm Diameter and With a Surface Absorptivity of 0.023

κ = diffusivity (cm^2/sec)

Equation 7 with the coefficients of equation 6 yields a diffusion time of 0.23 msec. An analgous radial diffusion time, τ_r, can also be defined in terms of the laser focal spot radius, r.

$$\tau_r = \frac{r^2}{4\kappa} \tag{8}$$

One expects that if the diffusion time τ_d is much less than the radial diffusion time τ_r then a back surface temperature measurement will be proportional to the absorbed energy. For our focal spot radius of 0.126 cm, the radial diffusion time is approximately 20 times larger than the axial heat diffusion time.

From the results of the above calcualtions, one expects to accurately determine the deposited energy density profile by measuring the time dependent temperature at the rear surface of a "thin" target as discussed previously. Table 3 shows several representative energy density profiles corresponding to the indicated temporal variation of temperature at r = 0. It is interesting to note that all possible energy density profiles yield the same asymptotic variation of temperature versus time.

$$\lim_{t\to\infty} T = \left(\frac{E_{ABS}}{4\pi KD}\right)\frac{1}{t} \tag{9}$$

where E_{ABS} is the total energy absorbed by the target.

It should be noted that Equation (9) is valid only for large radius targets in which the radial diffusion time is short enough to ignore any other loss terms (such as convection).

Figure 28 shows the relative variation of temperature with time as dependent on the selected energy density distributions. Curve (4), corresponding to the "doughnut" mode, is plotted for a ratio of outer to inner diameter of $\sqrt{2}$. For this case, the temperature peaks at a time, t_{peak}, given by

TABLE 3

CORRESPONDING ENERGY DENSITY

PROFILES AND TEMPERATU%ES AT r = 0

	Laser Energy	Energy Profiles	Temperature at r = 0
1	$E = \pi\delta^2 e_o$	$e = e_o e^{-r^2/\delta^2}$	$\frac{T_o}{(1 + t/\tau)}$ $T_o = \frac{e_o}{DC}$ $\tau = \frac{\delta^2}{4\kappa}$
2	$E = \pi d^2 e_o$	$e = e_o$ for $o<r<d$ $e = 0$ for $r<d$	$T_o \{1 - e^{-\tau/t}\}$ $\tau = d^2/4\kappa$
3	$E = \frac{\pi d^2}{2} e_o$	$e = e_o (1 - r^2/d^2)$ $e = 0$ for $r>d$	$T_o \{1 - \frac{t}{\tau}(1-e^{-\tau/t})\}$ $\tau = d^2/4\kappa$
4	$E = \pi e_o (\frac{d_2^2}{2} - d_1^2)$	$e = 0$, $o<r<d_1$ $e = e_o$, $d_1<r<d_2$ $e = 0$ $r>d_2$ (doughnut mode)	$T_o \{e^{-\tau_1/t} - e^{-\tau_2/t}\}$ $\tau_1 = d_1^2/4\kappa$, $\tau_2 = d_2^2/4\kappa$

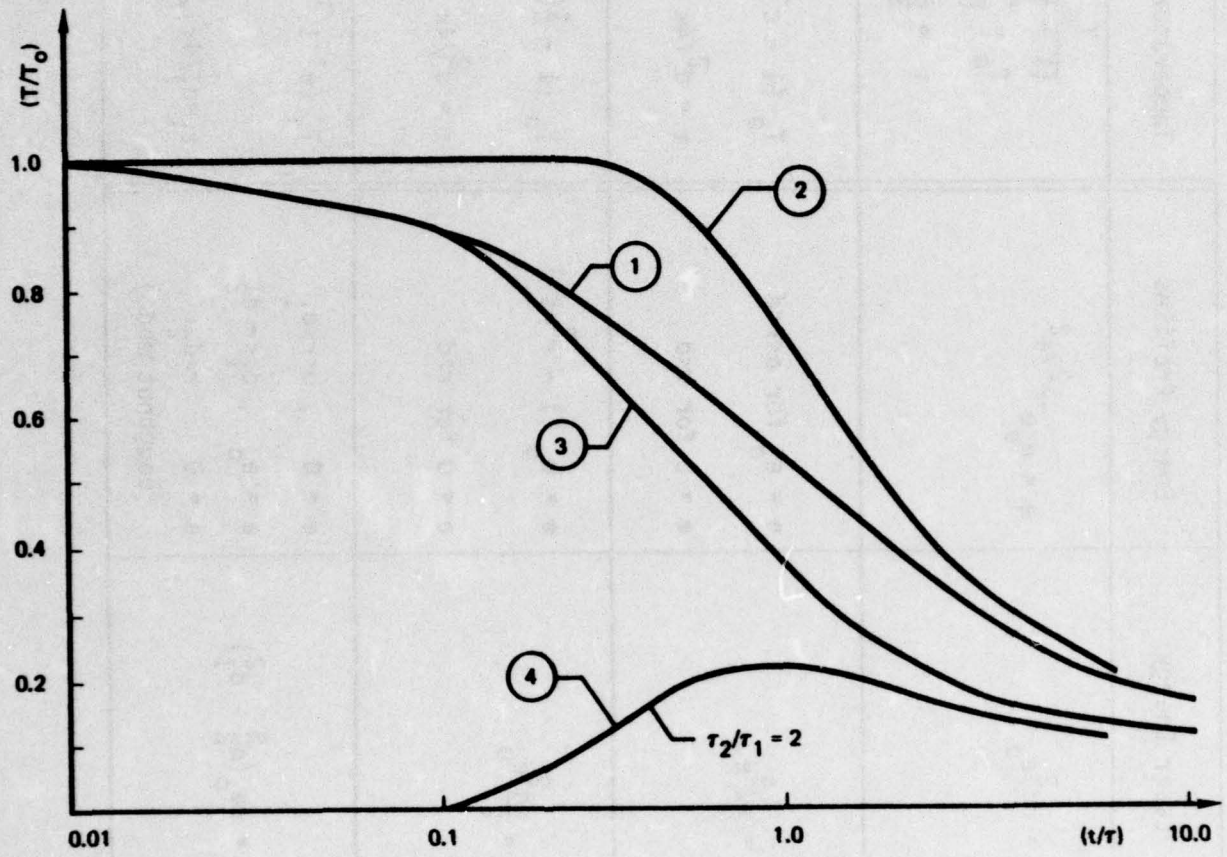


Figure 28. Temperature Versus Time for Selected Energy Density Profiles

$$t_{peak} = \frac{(\tau_2 - \tau_1)}{\ln(\tau_2/\tau_1)} \tag{10}$$

with a corresponding temperature maximum T_{max} determined by

$$\frac{T_{Max}}{T_o} = \left(\frac{\tau_2}{\tau_1} - 1\right)\left(\frac{\tau_2}{\tau_1}\right)^{-\tau_2/(\tau_2-\tau_1)} \tag{11}$$

It should be noted that all the energy modes with a maximum at r = 0 (curves (1), (2) and (3)) have a maximum temperature at t = 0.

Following the procedures indicated above, a series of experiments was performed in order to determine the energy density profile under conditions of "enhanced coupling." Usually, this means that LSD waves were ignited. The targets used were 2024-T3 aluminum alloy discs of 5 cm diameter with the following properties as determined by Touloukian (Ref. 23).

$C = 2.34$ joules/cm^3/^{o} C

$\kappa = 0.54$ cm^2/sec

$D = 0.028$ cm (target thickness)

$d = 0.126$ cm (laser spot radius)

The back surface temperature at r = 0 (at the center of the laser spot) was monitored with a 0.005 inch diameter chromel-alumel thermocouple spot-welded to the target.

Figure 29, for a low laser energy pulse and with no plasma production, shows the rear surface temperature. The solid curve, corresponding to case 3 of Table 3, was plotted using the known thermal properties of the target, the known focal radius, and the measured incident laser energy (E_{inc} = 1.42 joules). It should be recalled, for reference purposes, that

$$T_o = \frac{e_o}{DC} \tag{12}$$

The circled points of figure 29 are measured temperatures as indicated by the thermocouple. At early times the data do not agree with the theory

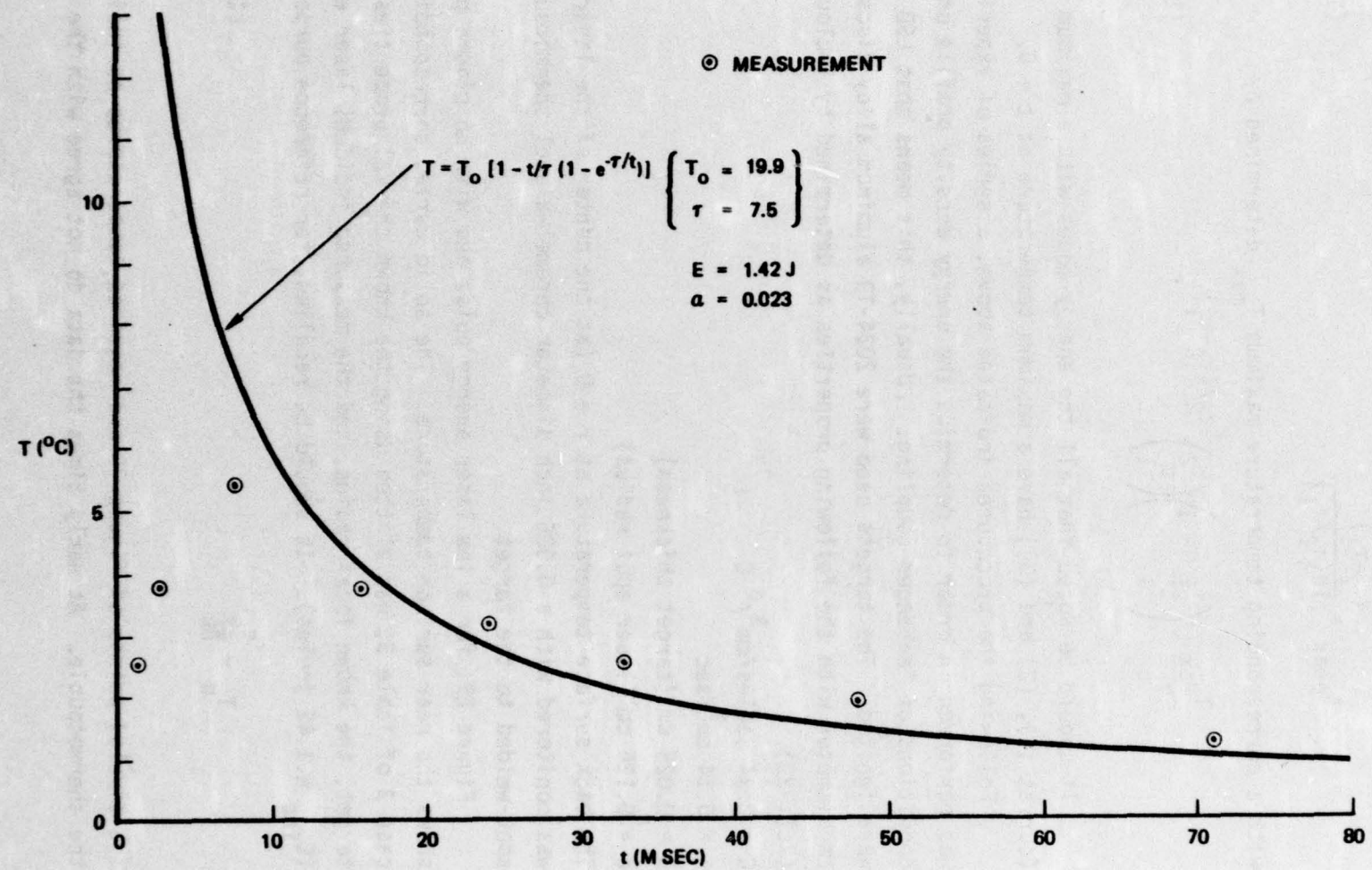


Figure 29. Comparison of Theory and Experiment for a Low Energy Laser Pulse (No Plasma Produced)

because of the relatively large time constant of this particular thermocouple which is approximately 5 to 7 msec and consequently cannot follow the early-time temperature history. Note the overall good comparison between theory and experiment for times greater than about 10 milliseconds. This is important since there were no "adjustable" parameters in the theory.

It is evident from previous work that the hot gas that results when LSD waves are ignited spreads over a considerably larger area than the focal spot itself. This is seen in figure 30 where again the rear surface temperature of a thin target is measured. The circled points represent data while the solid line is a theoretical curve which was fit at two points (in time) to match a Gaussian deposition of energy. The initial temperature T_o and the radial time constant τ were determined to be

$$T_o = 41^o \text{ K}$$
$$\tau = 90.8 \text{ msec} \qquad (13)$$

It should be noted by comparison with figure 29 that both the time scale for temperature decay and the temperature itself are considerably greater in this case when plasma was produced. It is clear that a Gaussian energy profile is a good representation of the absorbed energy profile. As of yet, the mathematical and numerical procedure needed to invert Equation 3 have not been developed so that temperature numerical data can be input into a computer program and a uniquely determined energy density profile determined. For the results of figure 30, the maximum absorbed energy density was determined to be

$$e_o = 2.70 \text{ joules/cm}^2$$

corresponding to a total absorbed energy of 1.63 joules. The total absorptivity was then determined to be

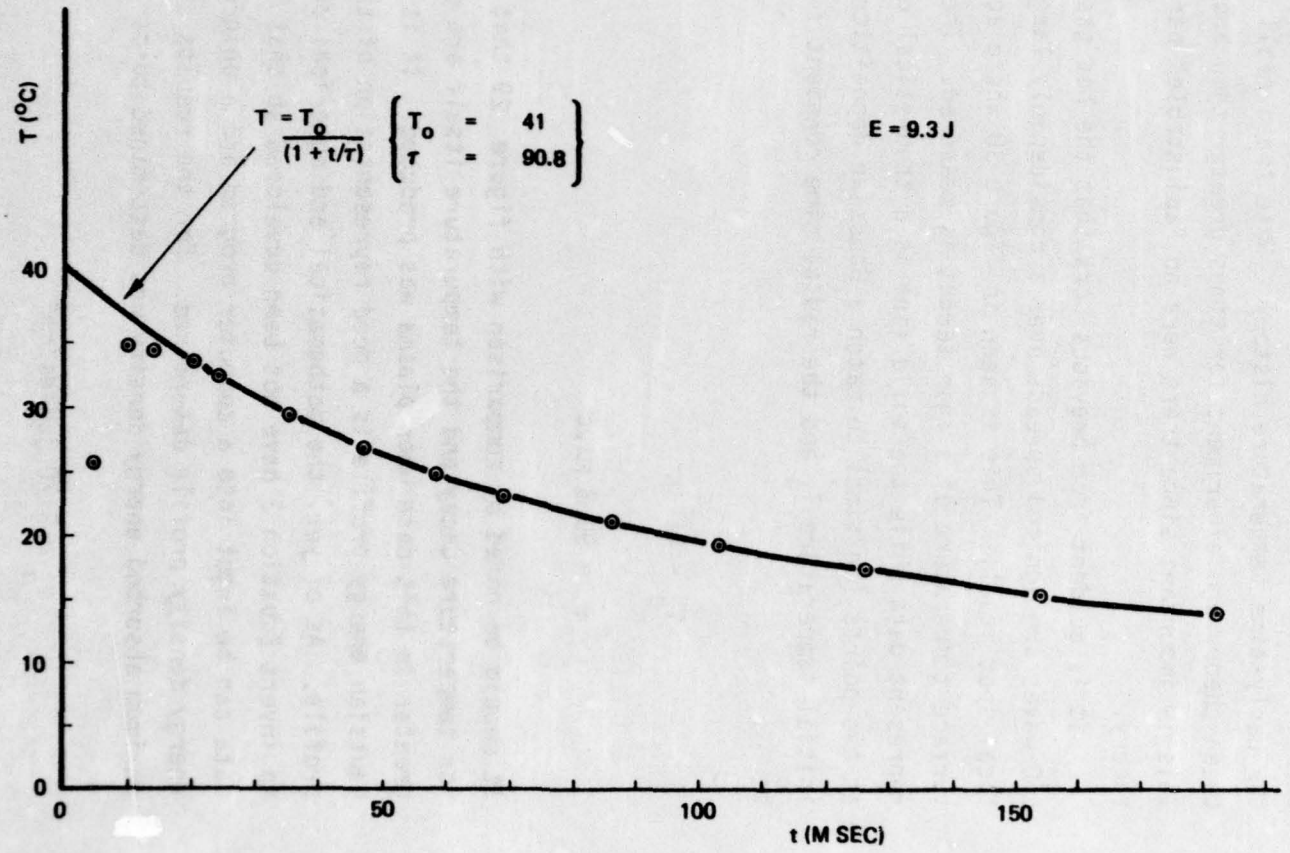


Figure 30. Temperature Versus Time Produced by a High-Energy Laser Pulse Which Produced a Laser-Supported Detonation Wave

$$\alpha = \frac{1.63}{9.3} = 0.175 \qquad (14)$$

The above data have assumed a Gaussian energy density profile which is reasonable for a "smooth" energy addition arising from plasma. It is possible, however, to fit the data to a cruder representation of the energy profile such as curve (2) of figure 28. In this case, the energy density is constant out to a radius to be determined. One finds (by fitting data at t = 20 and 86 milliseconds as done previously) that

$$\begin{aligned} T_o &= 34.2^o \text{ C} \\ \tau &= 82.4 \text{ milliseconds} \\ d &= 0.42 \text{ cm} \end{aligned} \qquad (15)$$

The corresponding absorbed energy was found to be 1.26 joules with a calculated absorptivity of $\alpha = 0.14$. The actual differences between the theoretical and experimental curves in this case, however, are considerably greater than in the previously considered Gaussian energy density profile. For this reason, a Gaussian approximation is believed to be more realistic.

Figure 31 shows the actual absorbed energy density profiles obtained both at low intensities (no plasma) and at intensities of the order of 2×10^7 watts/cm^2 where LSD waves are produced. In figure 31, the incident laser energy (in joules) is given for each case and one determines that 6.55 times as much energy was incident in the higher energy case. The parameter δ is the Gaussian width of the absorbed energy profile.

6. DAMAGE MODEL BASED ON THERMAL COUPLING MEASUREMENTS

The greatly enhanced energy deposition area on the target leads to a need for careful evaluation of the actual damage mechanisms available with enhanced coupling. This can be seen from figures 30 and 31 where the ratio of peak absorbed energy density at r = 0 (or target temperature)

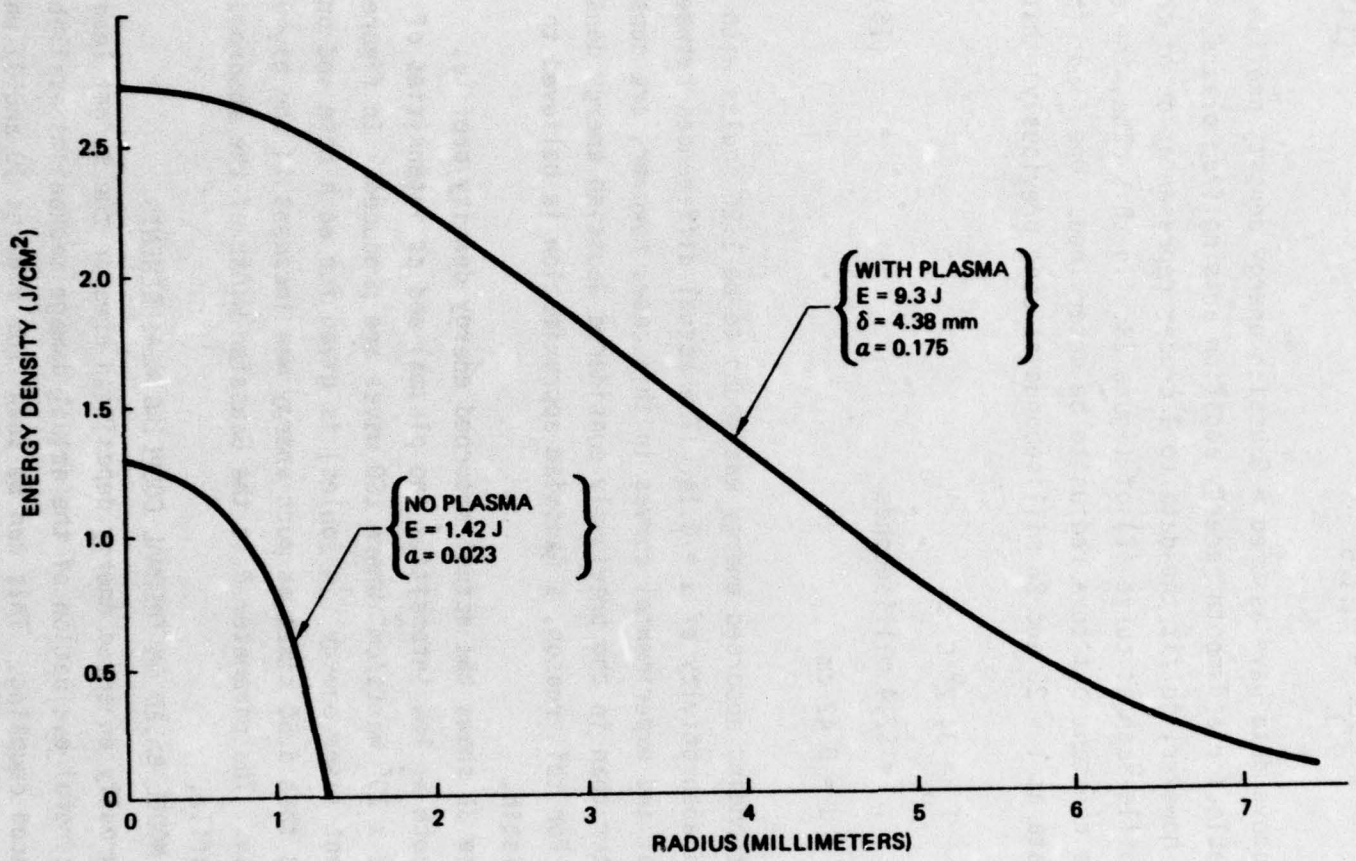


Figure 31. Comparison of the Absorbed Energy Density Profiles Obtained Both With and Without Plasma Production

was found to be only 2.06. As previously indicated, if no plasma interaction effects occurred, this ratio would have been 6.55 in order to be proportional to incident laser energies.

Thus, with these "small spot" experiments, it appears that high intensity laser beams, which produce LSD waves, would actually take a longer time and, hence, need more total delivered laser energy to burn through a target than at somewhat lower intensities. This effect can be seen in figure 32 which shows schematically the total laser energy W_L required to melt through a 3 mm thick slab of aluminum. For peak intensities less than approximately 10^7 watts/cm^2, the necessary delivered laser energy is constant and independent of intensity. Since the heat of fusion of aluminum is H = 1050 joules/cm^3, one finds

$$W_L \simeq \frac{DH}{\alpha} \simeq 12.5 \times 10^3 \text{ joules/cm}^2 \qquad (16)$$

If the absorptivity really increased to approximately 0.18 as indicated by the measurements, the laser energy to melt through the same slab would be

$$W_L = 1690 \text{ joules/cm}^2 \qquad (17)$$

This decrease, by a factor of about 7, in the laser energy required to melt through a given target would be a very important consideration in using high intensity pulsed lasers.

The above "enhanced" value of α is, in fact, the ratio of total absorbed energy divided by the incident laser energy. Since the actual area over which absorption takes place is very large compared to the beam area, however, the local absorptivity α_L is found to actually decrease compared to the intrinsic absorptivity. The value of α_L, near ignition threshold, is actually about $\alpha_L \simeq 0.0073$ at r = 0 and corresponds to the conditions shown in figure 31. The corresponding energy needed to melt through the aluminum plate under these conditions actually is found to increase by a factor of about 3.

The data presented above are based entirely on small spot 10.6 micron experiments. It should be noted, however, that Marcus (Ref. 24) has

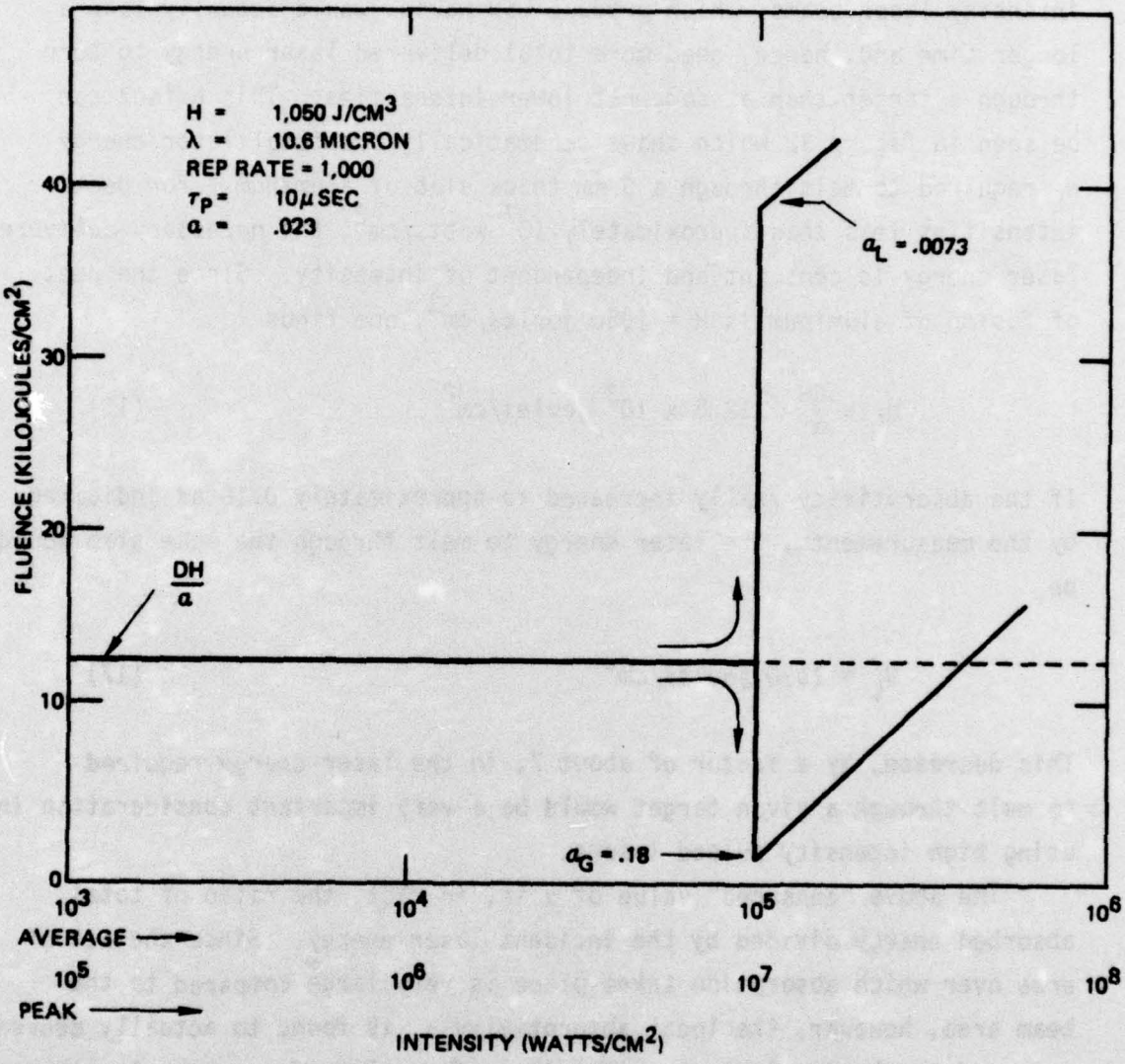


Figure 32. Fluence Required for Burnthrough of an 0.3CM Aluminum Plate

measured large spot thermal coupling with a pulsed CO_2 laser and has concluded, in contradiction to the above data, that most of the absorbed energy is, in fact, absorbed over the focal spot area itself. This discrepancy points out the need for further experiments in this area.

VII SUMMARY

It appears that the previously measured enhanced impulse production, (Ref. 5), which was obtained with double pulse laser beams on lead targets does not occur with more reflective targets. In the experiments reported here for both aluminum and stainless steel no optimum pulse separation was obtained. This conclusion was also confirmed by the lack of an observable pressure pulse produced by the second laser beam.

The gross thermal coupling coefficient of aluminum has been measured and an overall enhancement of about a factor of nine was found when plasmas were ignited with a CO_2 laser beam. This coupling coefficient exhibited a maximum however, and for larger laser energies decreased as E^{-1}. This dependence means that the target temperature is constant at high laser energies. Although the coupling coefficient increases at the enhancement threshold, measurement of the area on the target where coupling occurred indicated the specific coupling coefficient decreased for the case of plasma ignition. At least for the small laser spots used, the plasma spreads over the target surface and leads to heating over areas much larger than the focal area itself.

Thermal coupling measurements with double pulse lasers, as a simulation of repetitively pulsed effects, showed no optimum pulse separation. This indicates that no critical repetition rate dependence of thermal coupling can be expected from high average power lasers.

REFERENCES

1. Hall, R.B.,Maher, W.E., and Wei, P.S.P., "An Investigation of Laser Supported Detonation Waves," Boeing Aerospace Company Final Report on Contract F29601-72-C-0064, AFWL-TR-73-28, 1973.

2. Rudder, R.R., And Augostini, A.L. "Thermal Deposition Experiments with Microsecond Duration CO_2 Laser Radiation, R.R. Rudder, "Further Experimental Observations of the Interaction of Pulsed Five-Micron Radiation with Solid Matter," p. 197, Laser Digest-AFWL-TR-229, Oct. 1975.

3. Walters, C.T.,Barnes, R.H., and Beverly, R.W., III., "An Investigation of Mechanisms of Initiation of Laser-Supported Absorption (LSA) Waves," Battelle Columbus Laboratories, Final Report on Contract DAAH01-73-A-0776, 1975.

4. Conrad, R.W., "Laser-Target Interaction: Thermal Effects", J. of Defense Research, Series A, Vol. 4A, NO. 1, May 1975, pp. 433-438.

5. Hall, R.B.,Maher, W.E., and Nelson,D.J.,"Double-Pulse Laser Interaction Experiments," Boeing Aerospace Company Final Report on Contract F29601-73-G-0085, 1974.

6. Wei, P.S.P., Hall, R.B., and Maher, W.E., "Study of Laser-Supported Detonation Waves by Time-Resolved Spectroscopy," J. Chem. Phys. 59, 3692, 1974.

7. Eriksson, K.B.S., "Spectrum of the Singly Ionized Nitrogen Atom," Arkiv Foer Fysik 13, 303, 1958.

8. Wei, P.S.P., Hall, R.B., and Maher, W.E., "Study of Laser-Supported Detonation Waves by Time-Resolved Spectroscopy," J. Chem. Phys. 59, 3692, 1973.

9. Olme, A., "Spectrum of Singly Ionized Boron BII," Physica Scripta 1, 256, 1970.

10. Olem, A., "Spectrum of Doubly Ionized Boron, BIII," Arkiv Foer Fysik 40, 35, 1969.

11. Edlen, B., "The Term Analysis of Atomic Spectra," Physica Scripta 7, 93, 1973.

12. Langmuir I.,Lones, H.A., and Mackey, G.M.J., Phys. Rev 30, 201, 1927.

13. Chang, D.B. Drummond, J.E., and Hall, R.B., J. Appl. Phys. 41, 4851, 1970.

14. "Properties of Selected Commercial Glasses," Corning Glass Works, Corning, New York, 1965.

15. Bondarenko, B.V., Bufetov, I.A., and Schuka, A.A., "Energy of Electrons Emitted by the Laser Heated Surface of Metals," Phys. Lett. 45a, 251, 1973.

16. Lowder, J.E., and Pettingill, L.C., "Double-Pulse Pressure and Impulse Measurements," Lincoln Laboratory Optics Research No. 2, 1973, (April 24, 1974) p. 29.

17. Maher, W.E., Hall, R.B., and Johnson, R.R., "Experimental Study of Ignition and Propagation of Laser-Supported Detonation Waves," J. Appl. Phys. 45, 2138, 1974.

18. Pirri, A.N., Phys. Fluids 16, 1435, 1973.

19. Rudder, R.R., and Carlson, R.L., Material Response to Repetitively Pulsed 10.6 Micron Laser Radiation," Air Force Weapons Laboratory Laser Division Digest, Spring 1974.

20. Gilbert, K.G. and Carlson, R.L., "A Comparative Experimental Study of Material Interaction for Repetitively Pulsed and Continuous Wave CO_2 Lasers," Air Force Weapons Laboratory Report AFWL-TR-72-168, November 1972.

21. Byron, S., Klosterman, L., and Hall, R.B., "Laser-Supported Absorption Waves," J. Defense Research 4A, 468, 1975.

22. Ready, J.F., Effects of High-Power Laser Radiation, Academic Press, New York, 1971.

23. Thermophysical Properties of Materials, edited by Touloukian, Y.S., IFI/Plenum Press, New York, 1970, p. 1015.

24. Marcus, S., Lowder, J.E., Mooney, D.L., "Large Spot Thermal Coupling Measurements," Lincoln Laboratories Report MS-4042, July, 1975.